A modular, operator-splitting scheme for fluid–structure interaction problems with thick structures

M. Bukač[1], S. Čanić[2,*,†], R. Glowinski[2], B. Muha[3] and A. Quaini[2]

[1]*Department of Mathematics, University of Pittsburgh, Pittsburgh, PA, USA*
[2]*Department of Mathematics, University of Houston, Houston, TX, USA*
[3]*Department of Mathematics, University of Zagreb, Zagreb, Croatia*

SUMMARY

We present an operator-splitting scheme for fluid–structure interaction (FSI) problems in hemodynamics, where the thickness of the structural wall is comparable to the radius of the cylindrical fluid domain. The equations of linear elasticity are used to model the structure, while the Navier–Stokes equations for an incompressible viscous fluid are used to model the fluid. The operator-splitting scheme, based on the Lie splitting, separates the elastodynamics structure problem from a fluid problem in which structure inertia is included to achieve unconditional stability. We prove energy estimates associated with unconditional stability of this modular scheme for the full nonlinear FSI problem defined on a moving domain, without requiring any sub-iterations within time steps. Two numerical examples are presented, showing excellent agreement with the results of monolithic schemes. First-order convergence in time is shown numerically. Modularity, unconditional stability without temporal sub-iterations, and simple implementation are the features that make this operator-splitting scheme particularly appealing for multi-physics problems involving FSI. Copyright © 2013 John Wiley & Sons, Ltd.

1. INTRODUCTION

Fluid–structure interaction (FSI) problems arise in many applications. They include multi-physics problems in engineering such as aeroelasticity and propeller turbines, as well as biofluidic application such as self-propulsion organisms, fluid–cell interactions, and the interaction between blood flow and cardiovascular tissue. In biofluidic applications, such as the interaction between blood flow and cardiovascular tissue, the density of the structure (arterial walls) is roughly equal to the density of the fluid (blood). In such problems, the energy exchange between the fluid and the structure is significant, leading to a highly nonlinear FSI coupling. A comprehensive study of these problems remains to be a challenge because of their strong nonlinearity and multi-physics nature.

The development of numerical solvers for FSI problems has become particularly active since the 1980s [1–25].

Until recently, only monolithic algorithms seemed applicable to blood flow simulations [25–30]. These algorithms are based on solving the entire nonlinear coupled problem as one monolithic system. They are, however, generally quite expensive in terms of computational time, programming time, and memory requirements, as they require solving a sequence of strongly coupled problems using, for example, the fixed point and Newton's methods [13, 27, 31–34].

---

*Correspondence to: S. Čanić, Department of Mathematics, University of Houston, Houston, TX, USA.
†E-mail: canic@math.uh.edu

The multi-physics nature of the blood flow problem strongly suggests to employ partitioned (or staggered) numerical algorithms, where the coupled FSI problem is separated into a fluid sub-problem and a structure sub-problem. The fluid and structure sub-problems are integrated in time in an alternating way, and the coupling conditions are enforced asynchronously. When the density of the structure is much larger than the density of the fluid, as is the case in aeroelasticity, it is sufficient to solve, at every time step, just one fluid sub-problem and one structure sub-problem to obtain a solution. The classical loosely coupled partitioned schemes of this kind typically use the structure velocity in the fluid sub-problem as Dirichlet data for the fluid velocity (enforcing the no-slip boundary condition at the fluid–structure interface), while in the structure sub-problem, the structure is loaded by the fluid normal stress calculated in the fluid sub-problem. These Dirichlet–Neumann loosely coupled partitioned schemes work well for problems in which the structure is much heavier than the fluid. Unfortunately, when fluid and structure have comparable densities, which is the case in the blood flow application, the simple strategy of separating the fluid from the structure suffers from severe stability issues [35, 36]. This is because the energy of the discretized problem in Dirichlet–Neumann loosely coupled schemes does not approximate well the energy of the continuous problem. A partial solution to this problem is to sub-iterate several times between the fluid and structure sub-solvers at every time step until the energy of the continuous problem is well approximated. These strongly coupled partitioned schemes, however, are computationally expensive and may suffer from convergence issues for certain parameter values [35].

To get around these difficulties, and to retain the main advantages of loosely coupled partitioned schemes such as modularity, simple implementation, and low computational costs, several new loosely coupled algorithms have been proposed recently. In general, they behave quite well for FSI problems containing a thin fluid–structure interface with mass [17, 27, 32, 37–49].

For FSI problems in which the structure is 'thick', that is, the thickness of the structure is comparable to the transverse dimension of the fluid domain, partitioned, loosely coupled schemes are more difficult to construct. In fact, to the best of our knowledge, there have been no loosely coupled, partitioned schemes proposed so far in literature for a class of FSI problems in hemodynamics that contain thick structure models to study the elastodynamics of arterial walls. The closest works in this direction include a strongly coupled partition scheme by Badia *et al.* in [50] and an explicit scheme by Burman and Fernández where certain 'defect-correction' sub-iterations are necessary to achieve optimal accuracy [51].

More precisely, in [50], the authors construct a strongly coupled partitioned scheme based on certain Robin-type coupling conditions. In addition to the classical Dirichlet–Neumann and Neumann–Dirichlet schemes, they also propose Robin–Neumann and Robin–Robin schemes that converge without relaxation, and need a smaller number of sub-iteration between the fluid and the structure in each time step than classical strongly coupled schemes.

In [51], Burman and Fernández proposed an explicit scheme where the coupling between the fluid and a thick structure is enforced in a weak sense using Nitsche's approach [52]. The formulation in [51] still suffers from stability issues related to the added mass effect, which were corrected by adding a weakly consistent penalty term that includes pressure variations at the interface. The added term, however, lowers the temporal accuracy of the scheme, which was then corrected by proposing a few defect-correction sub-iterations to achieve optimal accuracy.

In the work presented here, we take a different approach to separate the calculation of the fluid and structure sub-problems in the case when the FSI problem incorporates a thick elastic structure. Our approach is based on the Lie splitting, also known as the Marchuk–Yanenko scheme. This splitting is applied to the coupled FSI problem written in arbitrary Lagrangian–Eulerian (ALE) form. Namely to deal with the motion of the fluid domain, in this manuscript, we utilize an ALE approach [11–17]. Once the coupled problem is written in ALE form, the Lie splitting is applied. The coupled FSI problem in ALE form is split into a fluid sub-problem and a structure sub-problem. The fluid sub-problem includes structure inertia to avoid instabilities associated with the added mass effect in partitioned schemes. This also avoids the need for any sub-iterations in each time step. A structure elastodynamics problem is then solved separately. We first introduced this approach in [40] to deal with FSI problems containing thin structures, leading to a completely partitioned, loosely coupled scheme called the kinematically coupled scheme. To increase the accuracy of the kinematically

coupled scheme, in [38], we introduced a modification of this scheme, called the kinematically coupled β-scheme, which was based on including a β-fraction of the pressure at the fluid–structure interface into the structure sub-problem. Another novelty of [38] was the fact that this scheme was applied to an FSI problem where the structure was modeled by the Koiter shell model accounting for both radial and longitudinal displacements. Because of its simple implementation, modularity, and good performance, modifications of this scheme have been used by several authors to study FSI problems in hemodynamics including cardiovascular stents (Muha and Čanić (2013), unpublished data), thin structures with longitudinal displacement [39], multi-layered structure of arterial walls, Bukač *et al.* (2013), unpublished data [53], poroelastic arterial walls (Bukač *et al.* (2013), unpublished data), or non-Newtonian fluids [54]. In the present paper, we extend the kinematically coupled β-scheme to FSI problems with thick structures.

This extension is not trivial because the resulting scheme, unlike those cited earlier, is not completely partitioned because in problems with thick structures, the *fluid–structure interface does not have a well-defined mass/inertia*. More precisely, to achieve unconditional stability, our operator-splitting strategy is based on including the fluid–structure interface inertia into the fluid sub-problem. This can be easily performed when the fluid–structure interface has mass. In that case, the structure inertia can be included in the fluid sub-problem through a Robin-type boundary condition at the fluid–structure interface [38]. However, in problems in which the interface between the fluid and structure is just a trace of a thick structure that is in contact with the fluid, as is the case in the present manuscript, the inclusion of the structure inertia in the fluid sub-problem is problematic if one wants to split the problem in the spirit of partitioned schemes. We address this issue by defining a new 'fluid sub-problem', which involves solving a *simplified coupled* problem on both the fluid domain and the structure domain, *in a monolithic fashion*. The inertia of the structure is included in this fluid sub-problem not through a boundary condition for the fluid sub-problem but by solving a simple, structure problem involving only structure inertia (and structural viscosity if the structure is *visco*elastic), coupled with the fluid problem via a simple continuity of stress condition at the interface. Although solving this simplified coupled problem on both domains is reminiscent of monolithic FSI schemes, the situation is, however, *much simpler*, as the *hyperbolic effects associated with fast wave propagation in the structural elastodynamics problem are not included here*. As a result, we show in Section 5.2.2 that the condition number of this sub-problem is smaller by several orders of magnitude than the condition number associated with monolithic FSI schemes. In fact, the condition number of this sub-problem is of the same order of magnitude as the condition number of the pure fluid sub-problem. Furthermore, the time step in this sub-problem can be taken larger than the time step in the classical monolithic schemes, which is dictated by the fast traveling waves in the elastic structure. Using this approach, we achieved unconditional stability of this operator-splitting scheme that separates the fluid from the structure sub-problems without a need for sub-iterations, but, as mentioned earlier, the drawback is the expense of generating the computational mesh on both the fluid and structure domains to resolve the fluid sub-problem.

In Section 4, we prove that for the fully nonlinear FSI problem defined on a moving domain, the proposed scheme satisfies an energy estimate that is associated with unconditional stability of the scheme, for all the parameters in the problem. To the best of our knowledge, this is the first result in which an energy estimate indicating unconditional stability of a partition-like scheme is obtained for a full nonlinear FSI problem.

In Section 5, we study two examples from literature involving FSI problems in hemodynamics with thick structures. We showed that in both cases, our simulations compared well with the results of monolithic schemes. Furthermore, in Section 5.2.1, we showed, on a numerical example, that our scheme is first-order accurate in time.

Although the presentation and numerical examples in this manuscript are given in terms of 2D problems, there is nothing in the operator-splitting scheme that depends on the dimension of the problem. Therefore, the same ideas as those presented in this manuscript apply to problems in 3D.

We conclude by emphasizing that, as in partitioned schemes, our scheme is modular in the sense that different modules can be easily added or replaced to study more complex multi-physics problems, and no sub-iterations between the different modules are needed to achieve stability.

Thus, we argue that the proposed operator-splitting scheme is closer in spirit to partitioned (loosely coupled) schemes than to monolithic schemes, providing an appealing approach to solve coupled FSI in hemodynamics with thick structures.

2. DESCRIPTION OF THE FLUID–STRUCTURE INTERACTION PROBLEM

We consider the flow of an incompressible, viscous fluid in a 2D channel of reference length L and reference width $2R$; see Figure 1. The lateral boundary of the channel is bounded by a thick, deformable wall with finite thickness h, that is, the wall thickness h is not necessarily small with respect to the channel radius R. We are interested in simulating a pressure-driven flow through a deformable 2D channel, in which the fluid and structure are fully coupled via a set of coupling conditions describing a two-way coupling. Without loss of generality, we consider only the upper half of the fluid domain supplemented by a symmetry condition at the axis of symmetry. Thus, the reference fluid and structure domains in our problem are given, respectively, by

$$\hat{\Omega}^f := \{(z, r)|0 < z < L, 0 < r < R\},$$
$$\hat{\Omega}^s := \{(z, r)|0 < z < L, R < r < R + h\},$$

with $\hat{\Gamma}$ denoting the Lagrangian boundary of $\hat{\Omega}^s$ in contact with the fluid

$$\hat{\Gamma} = (0, L).$$

Here, z and r denote the horizontal and vertical Cartesian coordinates, respectively (Figure 1). Throughout the rest of the manuscript, we will be using the 'hat' notation to denote the Lagrangian variables defined on the reference configuration.

The flow of an incompressible, viscous fluid is modeled by the Navier–Stokes equations:

$$\rho_f \left(\frac{\partial \boldsymbol{v}}{\partial t} + \boldsymbol{v} \cdot \nabla \boldsymbol{v} \right) = \nabla \cdot \boldsymbol{\sigma} \quad \text{in } \Omega^f(t) \text{ for } t \in (0, T), \tag{1}$$

$$\nabla \cdot \boldsymbol{v} = 0 \quad \text{in } \Omega^f(t) \text{ for } t \in (0, T), \tag{2}$$

where $\boldsymbol{v} = (v_z, v_r)$ is the fluid velocity, p is the fluid pressure, ρ_f is the fluid density, and $\boldsymbol{\sigma}$ is the fluid Cauchy stress tensor. For a Newtonian fluid, the Cauchy stress tensor is given by $\boldsymbol{\sigma} = -p\boldsymbol{I} + 2\mu_f \boldsymbol{D}(\boldsymbol{v})$, where μ_f is the fluid viscosity and $\boldsymbol{D}(\boldsymbol{v}) = (\nabla \boldsymbol{v} + (\nabla \boldsymbol{v})^\tau)/2$ is the rate-of-strain tensor.

The fluid domain $\Omega^f(t)$ is not known *a priori* as it depends on the solution of the problem. Namely the lateral boundary of $\Omega^f(t)$ is determined by the trace of the displacement of the thick structure at the fluid–structure interface, as it will be shown later.

At the inlet and outlet boundaries of the fluid domain, denoted by Γ_{in}^f and Γ_{out}^f, respectively, we prescribe the normal stress:

$$\boldsymbol{\sigma} \boldsymbol{n}_{\text{in}}^f(0, r, t) = -p_{\text{in}}(t)\boldsymbol{n}_{\text{in}}^f \quad \text{on } (0, R) \times (0, T), \tag{3}$$

$$\boldsymbol{\sigma} \boldsymbol{n}_{\text{out}}^f(L, r, t) = -p_{\text{out}}(t)\boldsymbol{n}_{\text{out}}^f \quad \text{on } (0, R) \times (0, T), \tag{4}$$
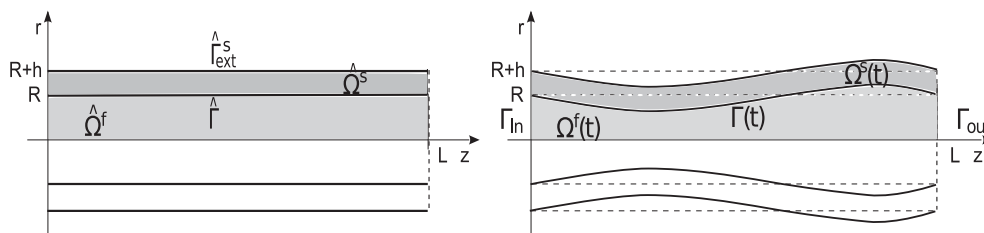

Figure 1. Left: reference domains $\hat{\Omega}^f \cup \hat{\Omega}^s$. Right: deformed domains $\Omega^f(t) \cup \Omega^s(t)$.

where $\boldsymbol{n}_{\text{in}}^{f}/\boldsymbol{n}_{\text{out}}^{f}$ are the outward normals to the inlet/outlet fluid boundaries, respectively. Even though not physiologically optimal, these boundary conditions are common in blood flow modeling [55–57].

At the bottom fluid boundary $r = 0$, denoted by Γ_b, the following symmetry conditions are prescribed:

$$\frac{\partial v_z}{\partial r}(z, 0, t) = 0, \quad v_r(z, 0, t) = 0 \quad \text{on } (0, L) \times (0, T). \tag{5}$$

The lateral fluid boundary is bounded by a deformable, 2D, elastic/viscoelastic wall with finite thickness, modeled by the following elastodynamics equations:

$$\rho_s \frac{\partial^2 \hat{U}}{\partial t^2} + \gamma \hat{U} = \nabla \cdot \boldsymbol{S}\left(\hat{U}\right) + \epsilon \Delta \frac{\partial \hat{U}}{\partial t} \quad \text{in } \hat{\Omega}^s \text{ for } t \in (0, T), \tag{6}$$

where $\hat{U}(\hat{z}, \hat{r}, t) = \left(\hat{U}_z(\hat{z}, \hat{r}, t), \hat{U}_r(\hat{z}, \hat{r}, t)\right)$ is the structure displacement, ρ_s is the structure density, and ϵ is the constant modeling viscoelastic structural effects. In the work described here, ϵ can be taken to be zero, thereby accounting for a possibility of modeling strictly elastic structures. The term $\gamma \hat{U}$ (i.e., the linearly elastic spring term) comes from 3D axial symmetry, accounting for the recoil due to circumferential strain, keeping the top and bottom structure displacements connected in 2D; see, for example, [47, 58, 59]. Tensor $\boldsymbol{S}$ is the first Piola–Kirchhoff stress tensor given by $\boldsymbol{S}\left(\hat{U}\right) = 2\mu_s \boldsymbol{D}\left(\hat{U}\right) + \lambda_s \left(\nabla \cdot \hat{U}\right) \boldsymbol{I}$, where μ_s and λ_s are the Lamé constants. The structure is described in the Lagrangian framework, defined on a fixed, reference domain $\hat{\Omega}^s$. In contrast, the fluid problem, written in the Eulerian framework, is defined on a domain $\Omega^f(t)$, which depends on time.

We assume that the structure is fixed at the inlet and outlet portions of the boundary:

$$\hat{U}(0, \hat{r}, t) = \hat{U}(L, \hat{r}, t) = 0, \quad \text{for } \hat{r} \in [R, R + h], t \in (0, T). \tag{7}$$

At the external structure boundary $\hat{\Gamma}_{ext}^s$, we assume that the structure is exposed to a certain external ambient pressure P_{ext}, while the axial displacement remains fixed:

$$\boldsymbol{n}_{ext}^s \cdot \boldsymbol{S} \boldsymbol{n}_{ext}^s = -P_{ext}, \quad \text{on } \hat{\Gamma}_{ext}^s \times (0, T), \tag{8}$$

$$\hat{U}_z = 0, \quad \text{on } \hat{\Gamma}_{ext}^s \times (0, T), \tag{9}$$

where $\boldsymbol{n}_{ext}^s$ is the outward unit normal vector on $\hat{\Gamma}_{ext}^s$.

Initially, the fluid and the structure are assumed to be at rest, with zero displacement from the reference configuration

$$\boldsymbol{v} = 0, \quad \hat{U} = 0, \quad \frac{\partial \hat{U}}{\partial t} = 0. \tag{10}$$

The fluid and structure are coupled via the kinematic and dynamic boundary conditions [60, 61]:

- *Kinematic coupling condition* describes continuity of velocity

$$\boldsymbol{v}\left(\hat{z} + \hat{U}_z(\hat{z}, R, t), R + \hat{U}_r(\hat{z}, R, t), t\right) = \frac{\partial \hat{U}}{\partial t}(\hat{z}, R, t) \quad \text{on } (0, L) \times (0, T). \tag{11}$$

- *Dynamic coupling condition* describes balance of contact forces:

$$J \widehat{\boldsymbol{\sigma} \boldsymbol{n}^f}\Big|_{\hat{\Gamma}} + \boldsymbol{S} \boldsymbol{n}^s|_{\hat{\Gamma}} + \epsilon \frac{\partial}{\partial \boldsymbol{n}^s}\left(\frac{\partial \hat{U}}{\partial t}\right)\Big|_{\hat{\Gamma}} = 0 \quad \text{on } (0, L) \times (0, T), \tag{12}$$

where J denotes the Jacobian of the transformation from the Eulerian to Lagrangian framework, $J = \sqrt{(1 + \partial \eta_z/\partial z)^2 + (\partial \eta_r/\partial z)^2}$, and $\widehat{\boldsymbol{\sigma} \boldsymbol{n}^f}$ denotes the normal fluid stress defined on $\hat{\Omega}^f = (0, L) \times (0, R)$ (here $\boldsymbol{n}^f$ is the outward unit normal to the deformed fluid domain), and $\boldsymbol{n}^s$ is the outward unit normal to the structural domain.
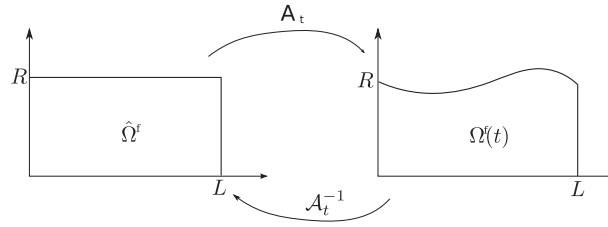
Figure 2. $\mathcal{A}_t$ maps the reference domain $\hat{\Omega}^f$ into the current domain $\Omega^f(t)$.

2.1. The ALE framework

To deal with the motion of the fluid domain, we adopt the ALE approach [11, 12, 57]. In the context of finite element method approximation of moving-boundary problems, the ALE method deals efficiently with the deformation of the mesh, especially near the interface between the fluid and the structure, and with the issues related to the approximation of the time derivatives $\partial v/\partial t \approx \left(v\left(t^{n+1}\right) - v(t^n)\right)/\Delta t$, which because $\Omega^f(t)$ depends on time, is not well defined because the values $v\left(t^{n+1}\right)$ and $v(t^n)$ correspond to the values of v defined at two different domains. The ALE approach is based on introducing a family of (arbitrary, invertible, smooth) mappings $\mathcal{A}_t$ defined on a single, fixed, reference domain $\hat{\Omega}^f$ such that, for each $t \in (t_0, T)$, $\mathcal{A}_t$ maps the reference domain $\hat{\Omega}^f = (0, L) \times (0, R)$ into the current domain $\Omega^f(t)$ (Figure 2):

$$\mathcal{A}_t : \hat{\Omega}^f \subset \mathbb{R}^2 \to \Omega^f(t) \subset \mathbb{R}^2, \quad x = \mathcal{A}_t(\hat{x}) \in \Omega^f(t), \quad \text{for } \hat{x} \in \hat{\Omega}^f.$$

In our approach, we define $\mathcal{A}_t$ to be a harmonic extension of the structure displacement $\hat{U}$ at the fluid–structure interface onto the whole domain $\hat{\Omega}^f$, for a given t :

$$\Delta \mathcal{A}_t = 0 \quad \text{in } \hat{\Omega}^f,$$

$$\mathcal{A}_t|_{\hat{\Gamma}} = \hat{U}|_{\hat{\Gamma}},$$

$$\mathcal{A}_t|_{\partial\hat{\Omega}^f \backslash \hat{\Gamma}} = 0.$$

To rewrite system (1)–(2) in the ALE framework, we notice that for a function $f = f(x, t)$ defined on $\Omega^f(t) \times (0, T)$, the corresponding function $\hat{f} := f \circ \mathcal{A}_t$ defined on $\hat{\Omega} \times (0, T)$ is given by

$$\hat{f}(\hat{x}, t) = f(\mathcal{A}_t(\hat{x}), t).$$

Differentiation with respect to time, after using the chain rule, gives

$$\frac{\partial f}{\partial t}\bigg|_{\hat{x}} = \frac{\partial f}{\partial t} + w \cdot \nabla f, \tag{13}$$

where w denotes domain velocity given by

$$w(x, t) = \frac{\partial \mathcal{A}_t(\hat{x})}{\partial t}. \tag{14}$$

Finally, system (1)–(2) in ALE framework reads as follows: find $v = (v_z, v_r)$ and p, with $\hat{v}(\hat{x}, t) = v(\mathcal{A}_t(\hat{x}), t)$ such that

$$\rho_f \left(\frac{\partial v}{\partial t}\bigg|_{\hat{x}} + (v - w) \cdot \nabla v \right) = \nabla \cdot \sigma, \qquad \text{in } \Omega^f(t) \times (0, T), \tag{15}$$

$$\nabla \cdot v = 0 \qquad \text{in } \Omega^f(t) \times (0, T), \tag{16}$$

with corresponding initial and boundary conditions.

We will apply the Lie splitting on this system written in ALE form. Before we do that, we introduce the notion of weak solutions to the coupled FSI problem. For this purpose, we utilize the ALE mapping, introduced earlier, and define the function spaces on moving domains in terms of the ALE-mapped functions, defined on the fixed, reference domain.

2.2. Weak solution of the coupled FSI problem

Define the following test function spaces

$$V^f(t) = \left\{ \boldsymbol{\varphi} : \Omega^f(t) \to \mathbb{R}^2 \mid \boldsymbol{\varphi} = \hat{\boldsymbol{\varphi}} \circ (\mathcal{A}_t)^{-1}, \hat{\boldsymbol{\varphi}} \in \left(H^1 \left(\hat{\Omega}^f \right) \right)^2, \varphi_r|_{r=0} = 0, \right\}, \quad (17)$$

$$Q(t) = \left\{ q : \Omega^f(t) \to \mathbb{R} \mid q = \hat{q} \circ (\mathcal{A}_t)^{-1}, \hat{q} \in L^2 \left(\hat{\Omega}^f \right) \right\}, \quad (18)$$

$$\hat{V}^s = \left\{ \hat{\boldsymbol{\psi}} : \hat{\Omega}^s \to \mathbb{R}^2 \mid \hat{\boldsymbol{\psi}} \in \left(H^1 \left(\hat{\Omega}^s \right) \right)^2, \hat{\boldsymbol{\psi}}|_{z=0,L} = 0, \hat{\psi}_z|_{\hat{\Gamma}^s_{ext}} = 0 \right\}, \quad (19)$$

for all $t \in [0, T)$ and introduce the following function space:

$$V^{fsi}(t) = \left\{ \left(\boldsymbol{\varphi}, \hat{\boldsymbol{\psi}} \right) \in V^f(t) \times \hat{V}^s \mid \boldsymbol{\varphi}|_{\Gamma(t)} = \hat{\boldsymbol{\psi}}|_{\hat{\Gamma}} \circ \left(\mathcal{A}_t^{-1}|_{\Gamma(t)} \right) \right\}. \quad (20)$$

The variational formulation of the coupled FSI problem now reads: For $t \in (0, T)$, find $(\boldsymbol{v}, \hat{\boldsymbol{U}}, p) \in V^f(t) \times \hat{V}^s \times Q(t)$ such that $\boldsymbol{v} = \hat{\boldsymbol{U}}_t \circ \mathcal{A}_t^{-1}$ on $\Gamma(t)$, and the following holds for all $(\boldsymbol{\varphi}, \hat{\boldsymbol{\psi}}, q) \in V^{fsi}(t) \times Q(t)$:

$$\rho_f \left\{ \int_{\Omega^f(t)} \frac{\partial \boldsymbol{v}}{\partial t} \cdot \boldsymbol{\varphi} d\boldsymbol{x} + \int_{\Omega^f(t)} (\boldsymbol{v} \cdot \nabla)\boldsymbol{v} \cdot \boldsymbol{\varphi} d\boldsymbol{x} \right\} + 2\mu_f \int_{\Omega^f(t)} \boldsymbol{D}(\boldsymbol{v}) : \boldsymbol{D}(\boldsymbol{\varphi}) d\boldsymbol{x}$$

$$- \int_{\Omega^f(t)} p \nabla \cdot \boldsymbol{\varphi} d\boldsymbol{x} + \rho_s \int_{\hat{\Omega}^s} \frac{\partial^2 \hat{\boldsymbol{U}}}{\partial t^2} \cdot \hat{\boldsymbol{\psi}} d\boldsymbol{x} + 2\mu_s \int_{\hat{\Omega}^s} \boldsymbol{D}(\hat{\boldsymbol{U}}) : \boldsymbol{D}(\hat{\boldsymbol{\psi}}) d\boldsymbol{x}$$

$$+ \lambda_s \int_{\hat{\Omega}^s} \left(\nabla \cdot \hat{\boldsymbol{U}} \right) \left(\nabla \cdot \hat{\boldsymbol{\psi}} \right) d\boldsymbol{x} + \gamma \int_{\hat{\Omega}^s} \hat{\boldsymbol{U}} \cdot \hat{\boldsymbol{\psi}} d\boldsymbol{x} + \epsilon \int_{\hat{\Omega}^s} \nabla \frac{\partial \hat{\boldsymbol{U}}}{\partial t} : \nabla \hat{\boldsymbol{\psi}} d\boldsymbol{x}$$

$$+ \int_{\hat{\Gamma}^s_{ext}} P_{ext} \left(\hat{\boldsymbol{\psi}} \cdot \boldsymbol{n}^s_{ext} \right) dS = \int_0^R p_{in}(t)\varphi_z|_{z=0} dr - \int_0^R p_{out}(t)\varphi_z|_{z=L} dr,$$

with

$$\int_{\Omega^f(t)} q \nabla \cdot \boldsymbol{v} d\boldsymbol{x} = 0.$$

3. THE NUMERICAL SCHEME

3.1. An operator-splitting approach

To solve the FSI problem written in ALE form (15)–(16), and with the initial and boundary conditions (3)–(12), we propose an operator-splitting scheme, which is based on the Lie operator splitting [62], also known as Marchuk–Yanenko splitting. The splitting is introduced to separate the different physics in the problem represented by the fluid and structure sub-problems. To achieve unconditional stability of such an approach, it is crucial to include inertia of the fluid–structure interface in the fluid sub-problem, thereby avoiding the 'added mass effect' responsible for instabilities of classical Dirichlet–Neumann partitioned schemes [35]. This can be easily performed when the

fluid–structure interface has mass, for example, the interface is modeled as a thin structure satisfying the Koiter shell equations, as was performed in [38, 40]. In that case, the structure inertia can be included in the fluid sub-problem through a Robin-type boundary condition at the fluid–structure interface [38]. However, in problems in which the interface between the fluid and structure is just a trace of a thick structure that is in contact with the fluid, as is the case in the present manuscript, the inclusion of structure inertia in the fluid sub-problem is problematic if one wants to split the problem in the spirit of partitioned schemes. We address this issue by defining a new fluid sub-problem, which involves solving a *simplified coupled* problem on both the fluid domain and the structure domain. The fluid sub-problem is solved *coupled with structure inertia* (and with the viscosity of the structure if the structure is viscoelastic) in a monolithic way, leaving out the elastic part of the structure. Although solving this simplified coupled problem on both domains is reminiscent of monolithic FSI schemes, the situation is, however, much simpler, because the hyperbolic effects associated with fast wave propagation in the structural elastodynamics problem are not included here. As a result, we show later in Section 5.2.2 that the condition number of this sub-problem is smaller by several orders of magnitude than the condition number associated with monolithic FSI schemes. In fact, the condition number of this sub-problem is of the same order of magnitude as the condition number of a pure fluid sub-problem! This approach also allows the choice of larger time steps, not restricted by the time scale associated with fast wave propagation in the elastic structure.

3.1.1. Lie splitting and the first-order system. The Lie operator splitting is defined for evolutionary problems, which can be written as a first-order system in time:

$$\frac{\partial \phi}{\partial t} + A(\phi) = 0, \quad \text{in } (0, T), \tag{21}$$

$$\phi(0) = \phi_0, \tag{22}$$

where A is an operator from a Hilbert space into itself, and A can be split, in a non-trivial decomposition, as

$$A = \sum_{i=1}^{I} A_i. \tag{23}$$

The Lie scheme consists of the following. Let $\Delta t > 0$ be a time discretization step. Denote $t^n = n\Delta t$, and let ϕ^n be an approximation of $\phi(t^n)$. Set $\phi^0 = \phi_0$. Then for $n \geqslant 0$, compute ϕ^{n+1} by solving

$$\frac{\partial \phi_i}{\partial t} + A_i(\phi_i) = 0 \quad \text{in } \left(t^n, t^{n+1}\right), \tag{24}$$

$$\phi_i(t^n) = \phi^{n+(i-1)/I}, \tag{25}$$

and then set $\phi^{n+i/I} = \phi_i\left(t^{n+1}\right)$, for $i = 1, \ldots, I$. This method is first-order accurate in time. More precisely, if (21) is defined on a finite-dimensional space, and if the operators A_i are smooth enough, then $\|\phi(t^n) - \phi^n\| = O(\Delta t)$ [62].

To apply the Lie operator-splitting scheme, we must rewrite system (1)–(12) in first-order form. For this purpose, we introduce the structure velocity $\hat{V} = \frac{\partial \hat{U}}{\partial t}$ and rewrite the problem as follows: find $\boldsymbol{v} = (v_z, v_r)$, p, $\hat{U} = \left(\hat{U}_z, \hat{U}_r\right)$ and $\hat{V} = \left(\hat{V}_z, \hat{V}_r\right)$, with $\hat{\boldsymbol{v}}(\hat{\boldsymbol{x}}, t) = \boldsymbol{v}(\mathcal{A}_t(\hat{\boldsymbol{x}}), t)$, such that

$$\rho_f \left(\left.\frac{\partial \boldsymbol{v}}{\partial t}\right|_{\hat{\boldsymbol{x}}} + (\boldsymbol{v} - \boldsymbol{w}) \cdot \nabla \boldsymbol{v} \right) = \nabla \cdot \boldsymbol{\sigma}, \quad \text{in } \Omega^f(t) \times (0, T), \tag{26}$$

$$\nabla \cdot \boldsymbol{v} = 0, \ \text{in } \Omega^f(t) \times (0, T), \tag{27}$$

$$\rho_s \frac{\partial \hat{V}}{\partial t} + \gamma \hat{U} = \nabla \cdot S\left(\hat{U}\right) + \epsilon \Delta \hat{V}, \text{ in } \hat{\Omega}_s \times (0, T), \tag{28}$$

$$\frac{\partial \hat{U}}{\partial t} = \hat{V}, \text{ in } \hat{\Omega}_s \times (0, T), \tag{29}$$

with the coupling conditions at the fluid–structure interface

$$\hat{V}|_{\hat{\Gamma}} = \hat{v}|_{\hat{\Gamma}}, \tag{30}$$

$$J \widehat{\sigma n^f}|_{\hat{\Gamma}} + S n^s|_{\hat{\Gamma}} + \epsilon \left.\frac{\partial \hat{V}}{\partial n^s}\right|_{\hat{\Gamma}} = 0, \tag{31}$$

(where $\hat{v}|_{\hat{\Gamma}}$ denotes $v\left(\hat{z} + \hat{U}_z\left(\hat{z}, R, t\right), R + \hat{U}_r\left(\hat{z}, R, t\right), t\right)$; and $\widehat{\sigma n^f}|_{\hat{\Gamma}}$ denotes the normal fluid stress defined on the reference fluid domain $\hat{\Omega}^f$), and with boundary conditions

$$\frac{\partial v_z}{\partial r}(z, 0, t) = v_r(z, 0, t) = 0 \quad \text{on } \Gamma_b^f, \tag{32}$$

$$v(0, R, t) = v(L, R, t) = 0, \quad \hat{U}|_{\hat{z}=0,L} = 0, \tag{33}$$

$$\sigma n_{\text{in}}^f(0, r, t) = -p_{\text{in}}(t) n_{\text{in}}^f, \tag{34}$$

$$\sigma n_{\text{out}}^f(L, r, t) = -p_{\text{out}}(t) n_{\text{out}}^f \text{ on } (0, R) \times (0, T). \tag{35}$$

$$n_{\text{ext}}^s \cdot S n_{\text{ext}}^s = -P_{\text{ext}} \quad \text{on } \hat{\Gamma}_{\text{ext}}^s \times (0, T), \tag{36}$$

$$\hat{U}_z = 0 \qquad \text{on } \hat{\Gamma}_{\text{ext}}^s \times (0, T). \tag{37}$$

At time $t = 0$, the following initial conditions are prescribed:

$$v|_{t=0} = \mathbf{0}, \quad \hat{U}|_{t=0} = \mathbf{0}, \quad \hat{V}|_{t=0} = \mathbf{0}. \tag{38}$$

Using the Lie operator-splitting approach, problem (26)–(38) is split into a sum of the following sub-problems:

A1. An elastodynamics sub-problem for the structure.
A2. A fluid sub-problem, coupled with structure inertia (and the viscous part of the structure equation if $\epsilon \neq 0$).

We will be numerically implementing this splitting by further splitting the fluid sub-problem into a dissipative part and a non-dissipative part. Namely we will be using the Lie splitting to separate the time-dependent Stokes problem from a pure advection problem. This way, one can use non-dissipative solvers for non-dissipative problems, thereby achieving higher accuracy. This is particularly relevant if one is interested in solving advection-dominated problems, such as transport of nano-particles by blood. However, this additional splitting is not necessary to achieve stability of the scheme, as we show in Section 4, where only problems A1 and A2 will be used to show an energy estimate associated with unconditional stability of the scheme. However, for completeness, we show in the next section the implementation of our numerical scheme in which the fluid sub-problem is further split into two, leading to the following Lie splitting of the coupled FSI problem:

A1. An elastodynamics sub-problem for the structure.
A2(a). A time-dependent Stokes problem for the fluid.
A2(b). A fluid and ALE advection problem.

3.1.2. Details of the operator-splitting scheme. Before we define each of the sub-problems mentioned earlier, we split the fluid stress $\widehat{\sigma}\mathbf{n}$ into two parts, parts I and II:

$$\widehat{\sigma}\mathbf{n} = \underbrace{\widehat{\sigma}\mathbf{n} + \beta\,\widehat{p}\widehat{\mathbf{n}}}_{(I)}\underbrace{-\beta\,\widehat{p}\widehat{\mathbf{n}}}_{(II)},$$

where β is a number between 0 and 1, $0 \leqslant \beta \leqslant 1$. Different values of β effect the accuracy of the scheme [38], but not stability (Čanić *et al.* (2013), unpublished data). For the problem discussed in the current manuscript, our experimental observations indicate that $\beta = 1$ provides the kinematically coupled β-scheme with highest accuracy.

In addition to the splitting of the fluid stress, we also separate different physical effects in the structure problem. We split the viscoelastic effects from the purely elastic effects and treat the structural viscoelasticity together with the fluid, while treating the pure elastodynamics of the structure in a separate, hyperbolic, structural sub-problem. Details of the splitting are as follows:

Problem A1: A pure elastodynamics problem is solved on $\hat{\Omega}^s$ with a boundary condition on $\hat{\Gamma}$ involving part II of the normal fluid stress. Thus, the structure elastodynamics is driven by the initial velocity of the structure (given by the fluid velocity at the fluid–structure interface from the previous time step) and by the fluid pressure loading $\beta J\widehat{(p\mathbf{n}^f)}$ acting on the fluid–structure interface (obtained from the previous time step). The problem reads: find $\boldsymbol{v}$, $\hat{\boldsymbol{U}}$, and $\hat{\boldsymbol{V}}$, with p^n and J^n obtained at the previous time step, such that

$$\begin{cases} \dfrac{\partial \boldsymbol{v}}{\partial t}\Big|_{\hat{\boldsymbol{x}}} = 0, \quad \text{in } \Omega^f(t^n) \times (t^n, t^{n+1}), \\[2mm] \rho_s \dfrac{\partial \hat{\boldsymbol{V}}}{\partial t} + \gamma \hat{\boldsymbol{U}} = \nabla \cdot \boldsymbol{S}\left(\hat{\boldsymbol{U}}\right), \quad \dfrac{\partial \hat{\boldsymbol{U}}}{\partial t}(z,t) = \hat{\boldsymbol{V}}, \quad \text{in } \hat{\Omega}^s \times (t^n, t^{n+1}), \\[2mm] -J^n \beta \left(\widehat{p^n \boldsymbol{n}^f}\right)\big|_{\hat{\Gamma}} + \boldsymbol{S}\boldsymbol{n}^s\big|_{\hat{\Gamma}} = 0, \quad \text{on } \hat{\Gamma} \times (t^n, t^{n+1}), \end{cases}$$

with boundary conditions

$$\hat{\boldsymbol{U}}\big|_{z=0,L} = 0,$$

$$\hat{U}_z = 0, \quad \boldsymbol{n}^s_{ext} \cdot \boldsymbol{S}\boldsymbol{n}^s_{ext} = -P_{ext} \quad \text{on } \hat{\Gamma}^s_{ext} \times (t^n, t^{n+1}),$$

and initial conditions

$$\boldsymbol{v}(t^n) = \boldsymbol{v}^n, \quad \hat{\boldsymbol{U}}(t^n) = \hat{\boldsymbol{U}}^n, \quad \hat{\boldsymbol{V}}(t^n) = \hat{\boldsymbol{V}}^n.$$

Then set $\boldsymbol{v}^{n+1/3} = \boldsymbol{v}(t^{n+1})$, $\hat{\boldsymbol{U}}^{n+1/3} = \hat{\boldsymbol{U}}\left(t^{n+1}\right)$, $\hat{\boldsymbol{V}}^{n+1/3} = \hat{\boldsymbol{V}}\left(t^{n+1}\right)$.
A new ALE velocity $\boldsymbol{w}^{n+1}$ is calculated based on the current and previous locations of the fluid domain: $\boldsymbol{w}^{n+1} = \partial \mathcal{A}_t / \partial t \ \left(\approx \left(\mathcal{A}_t^{n+1} - \mathcal{A}_t^n\right)/\Delta t\right)$.

Problem A2(a). A time-dependent Stokes problem is solved on the fixed fluid domain $\Omega^f(t^n)$, coupled with the viscous part of the structure problem defined on $\hat{\Omega}^s$. (For higher accuracy, $\Omega^f(t^n)$ can be replaced with $\Omega^f(t^{n+1})$.) The coupling is performed via the kinematic coupling condition and a portion of the dynamic coupling condition involving only part I of the fluid stress. When $\epsilon = 0$ (the purely elastic case), the problem on $\hat{\Omega}^s$ consists of only setting the structural velocity $\hat{\boldsymbol{V}}$ equal to the structural velocity from the previous time step, as $\partial \hat{\boldsymbol{V}} / \partial t = 0$ in this sub-problem. The problem reads as follows: Find $\boldsymbol{v}$, p, $\hat{\boldsymbol{V}}$, and $\hat{\boldsymbol{U}}$, with $\hat{\boldsymbol{v}}(\hat{\boldsymbol{x}}, t) = \boldsymbol{v}(\mathcal{A}_t(\hat{\boldsymbol{x}}), t)$,

such that for $t \in \left(t^n, t^{n+1}\right)$, with p^n and J^n obtained in the previous time step, the following holds:

$$
\begin{cases}
\rho_f \dfrac{\partial \boldsymbol{v}}{\partial t}\Big|_{\hat{\boldsymbol{x}}} = \nabla \cdot \boldsymbol{\sigma}, \quad \nabla \cdot \boldsymbol{v} = 0, \quad \text{in } \Omega^f(t^n) \times \left(t^n, t^{n+1}\right), \\[4mm]
\rho_s \dfrac{\partial \hat{\boldsymbol{V}}}{\partial t} = \epsilon \Delta \hat{\boldsymbol{V}}, \quad \dfrac{\partial \hat{\boldsymbol{U}}}{\partial t}(\hat{z}, t) = 0, \quad \text{in } \hat{\Omega}^s \times \left(t^n, t^{n+1}\right), \\[4mm]
J^{n+1} \widehat{\boldsymbol{\sigma} \boldsymbol{n}^f}\big|_{\hat{\Gamma}} + J^n \beta \left(\widehat{p^n \boldsymbol{n}^f}\right)\big|_{\hat{\Gamma}} + \epsilon \dfrac{\partial \hat{\boldsymbol{V}}}{\partial \boldsymbol{n}^s}\big|_{\hat{\Gamma}} = 0, \text{ on } \hat{\Gamma} \times \left(t^n, t^{n+1}\right), \\[4mm]
\hat{\boldsymbol{V}}|_{\hat{\Gamma}} = \hat{\boldsymbol{v}}|_{\hat{\Gamma}}, \text{ on } \hat{\Gamma} \times \left(t^n, t^{n+1}\right),
\end{cases}
$$

with the following boundary conditions on $\Gamma_{\text{in}}^f \cup \Gamma_{\text{out}}^f \cup \Gamma_b^f$:

$$
\frac{\partial v_z}{\partial r}(z, 0, t) = v_r(z, 0, t) = 0 \quad \text{on } \Gamma_b^f,
$$

$$
\boldsymbol{v}(0, R, t) = \boldsymbol{v}(L, R, t) = 0,
$$

$$
\boldsymbol{\sigma} \boldsymbol{n}_{\text{in}}^f = -p_{\text{in}}(t) \boldsymbol{n}_{\text{in}}^f \text{ on } \Gamma_{\text{in}}^f, \quad \boldsymbol{\sigma} \boldsymbol{n}_{\text{out}}^f = -p_{\text{out}}(t) \boldsymbol{n}_{\text{out}}^f \text{ on } \Gamma_{\text{out}}^f,
$$

and initial conditions

$$
\boldsymbol{v}(t^n) = \boldsymbol{v}^{n+1/3}, \quad \hat{\boldsymbol{U}}(t^n) = \hat{\boldsymbol{U}}^{n+1/3}, \quad \hat{\boldsymbol{V}}(t^n) = \hat{\boldsymbol{V}}^{n+1/3}.
$$

Then set $\boldsymbol{v}^{n+2/3} = \boldsymbol{v}(t^{n+1})$, $\hat{\boldsymbol{U}}^{n+2/3} = \hat{\boldsymbol{U}}(t^{n+1})$, $\hat{\boldsymbol{V}}^{n+2/3} = \hat{\boldsymbol{V}}(t^{n+1})$, $p^{n+1} = p(t^{n+1})$.

Problem A2(b): A fluid and ALE advection problem is solved on a fixed fluid domain $\Omega^f(t^n)$ with the ALE velocity $\boldsymbol{w}^{n+1}$ calculated in problem A1. (For higher accuracy, $\Omega(t^n)$ can be replaced by $\Omega(t^{n+1})$.) The problem reads as follows: find $\boldsymbol{v}$, $\hat{\boldsymbol{U}}$, and $\hat{\boldsymbol{V}}$ with $\hat{\boldsymbol{v}}(\hat{\boldsymbol{x}}, t) = \boldsymbol{v}(\mathcal{A}_t(\hat{\boldsymbol{x}}), t)$, such that for $t \in \left(t^n, t^{n+1}\right)$,

$$
\begin{cases}
\dfrac{\partial \boldsymbol{v}}{\partial t}\Big|_{\hat{\boldsymbol{x}}} + \left(\boldsymbol{v}^{n+2/3} - \boldsymbol{w}^{n+1}\right) \cdot \nabla \boldsymbol{v} = 0, \quad \text{in } \Omega^f(t^n) \times \left(t^n, t^{n+1}\right), \\[4mm]
\dfrac{\partial \hat{\boldsymbol{V}}}{\partial t}(\hat{z}, t) = 0, \quad \dfrac{\partial \hat{\boldsymbol{U}}}{\partial t}(\hat{z}, t) = 0, \quad \text{in } \hat{\Omega}^s \times \left(t^n, t^{n+1}\right),
\end{cases}
$$

with boundary conditions

$$
\boldsymbol{v} = \boldsymbol{v}^{n+2/3} \text{ on } \Gamma_-^{n+2/3}, \text{ where}
$$

$$
\Gamma_-^{n+2/3} = \left\{ \boldsymbol{x} \in \mathbb{R}^2 \,|\, \boldsymbol{x} \in \partial \Omega^f(t^n), \left(\boldsymbol{v}^{n+2/3} - \boldsymbol{w}^{n+1}\right) \cdot \boldsymbol{n}^f < 0 \right\},
$$

and initial conditions

$$
\boldsymbol{v}(t^n) = \boldsymbol{v}^{n+2/3}, \quad \hat{\boldsymbol{U}}(t^n) = \hat{\boldsymbol{U}}^{n+2/3}, \quad \hat{\boldsymbol{V}}(t^n) = \hat{\boldsymbol{V}}^{n+2/3}.
$$

Then set $\boldsymbol{v}^{n+1} = \boldsymbol{v}(t^{n+1})$, $\hat{\boldsymbol{U}}^{n+1} = \hat{\boldsymbol{U}}(t^{n+1})$, $\hat{\boldsymbol{V}}^{n+1} = \hat{\boldsymbol{V}}(t^{n+1})$.
Do $t^n = t^{n+1}$ and return to problem A1.

Remark 1
The method proposed earlier works well even if the fluid and structure steps are performed in reverse order.

3.2. Discretized sub-problems

In this section, we discretize each problem in space and time, and describe our solution strategy. To discretize the sub-problems in time, we sub-divide the time interval $(0, T)$ into N sub-intervals of width Δt. For the space discretization, we use the finite element method. Thus, for $t^n = n\Delta t, 0 \leqslant n \leqslant N$, we define the finite element spaces $V_h^f(t^n) \subset V^f(t^n), Q_h^f(t^n) \subset Q^f(t^n), V_h^{fsi}(t^n) \subset V^{fsi}(t^n)$ and $\hat{V}_h^s \subset \hat{V}^s$. To write the weak formulation, the following notation for the corresponding bilinear forms will be used:

$$a_f\left(\boldsymbol{v}, \boldsymbol{\varphi}^f\right) := 2\mu_f \int_{\Omega^f(t^n)} \boldsymbol{D}(\boldsymbol{v}) : \boldsymbol{D}\left(\boldsymbol{\varphi}^f\right) d\boldsymbol{x}, \tag{39}$$

$$b_f\left(p_f, \boldsymbol{\varphi}^f\right) := \int_{\Omega^f(t^n)} p_f \nabla \cdot \boldsymbol{\varphi}^f d\boldsymbol{x}, \tag{40}$$

$$a_v\left(\hat{\boldsymbol{V}}, \hat{\boldsymbol{\varphi}}^v\right) := \epsilon \int_{\hat{\Omega}^s} \nabla \hat{\boldsymbol{V}} : \nabla \hat{\boldsymbol{\varphi}}^v d\boldsymbol{x}, \tag{41}$$

$$a_e\left(\hat{\boldsymbol{U}}, \hat{\boldsymbol{\varphi}}^s\right) := 2\mu_s \int_{\hat{\Omega}^s} \boldsymbol{D}(\hat{\boldsymbol{U}}) : \boldsymbol{D}\left(\hat{\boldsymbol{\varphi}}^s\right) d\boldsymbol{x} + \lambda_s \int_{\hat{\Omega}^s} \left(\nabla \cdot \hat{\boldsymbol{U}}\right)\left(\nabla \cdot \hat{\boldsymbol{\varphi}}^s\right) d\boldsymbol{x}$$
$$+ \gamma \int_{\hat{\Omega}^s} \hat{\boldsymbol{U}} \cdot \hat{\boldsymbol{\varphi}}^s d\boldsymbol{x}. \tag{42}$$

Problem A1: To discretize problem A1 in time, we used the second-order Newmark scheme. The weak formulation of the fully discrete problem is given as follows: find $\hat{\boldsymbol{U}}_h^{n+1/3} \in \hat{V}_h^s$ and $\hat{\boldsymbol{V}}_h^{n+1/3} \in \hat{V}_h^s$ such that for all $(\hat{\boldsymbol{\varphi}}_h^s, \boldsymbol{\phi}_h^s) \in \hat{V}_h^s \times \hat{V}_h^s$, with p_h^n obtained at the previous time step:

$$\rho_s \int_{\hat{\Omega}^s} \frac{\hat{\boldsymbol{V}}_h^{n+1/3} - \hat{\boldsymbol{V}}_h^n}{\Delta t} \cdot \hat{\boldsymbol{\varphi}}_h^s d\boldsymbol{x} + a_e\left(\frac{\hat{\boldsymbol{U}}_h^n + \hat{\boldsymbol{U}}_h^{n+1/3}}{2}, \hat{\boldsymbol{\varphi}}_h^s\right) = J^n \beta \int_{\hat{\Gamma}} \widehat{p_h^n \boldsymbol{n}^f} \cdot \hat{\boldsymbol{\varphi}}_h^s d\boldsymbol{x},$$

$$\rho_s \int_{\hat{\Omega}^s} \left(\frac{\hat{\boldsymbol{V}}_h^n + \hat{\boldsymbol{V}}_h^{n+1/3}}{2} - \frac{\hat{\boldsymbol{U}}_h^{n+1/3} - \hat{\boldsymbol{U}}_h^n}{\Delta t}\right) \cdot \boldsymbol{\phi}_h^s d\boldsymbol{x} = 0.$$

Problem A2(a): We discretize problem A2(a) in time using the backward Euler method. The weak formulation of the fully discrete problem is given as follows: find $\left(\boldsymbol{v}_h^{n+2/3}, \hat{\boldsymbol{V}}_h^{n+2/3}, p_h^{n+2/3}\right) \in V_h^{fsi}(t^n) \times Q_h^f(t^n)$ such that for all $\left(\boldsymbol{\varphi}_h^f, \hat{\boldsymbol{\varphi}}_h^v, \psi_h^f\right) \in V_h^{fsi}(t^n) \times Q_h^f(t^n)$:

$$\rho_f \int_{\Omega^f(t^n)} \frac{\boldsymbol{v}_h^{n+2/3} - \boldsymbol{v}_h^{n+1/3}}{\Delta t} \cdot \boldsymbol{\varphi}_h^f d\boldsymbol{x} + a_f\left(\boldsymbol{v}_h^{n+2/3}, \boldsymbol{\varphi}_h^f\right) - b_f\left(p_h^{n+2/3}, \boldsymbol{\varphi}_h^f\right) + b_f\left(\psi_h^f, \boldsymbol{v}_h^{n+2/3}\right)$$

$$+ \rho_s \int_{\hat{\Omega}^s} \frac{\hat{\boldsymbol{V}}_h^{n+2/3} - \hat{\boldsymbol{V}}_h^{n+1/3}}{\Delta t} \cdot \hat{\boldsymbol{\varphi}}_h^v d\boldsymbol{x} + a_v\left(\hat{\boldsymbol{V}}_h^{n+2/3}, \hat{\boldsymbol{\varphi}}_h^v\right) = \int_0^R p_{\text{in}}\left(t^{n+1}\right) \varphi_{x,h}^f|_{x=0} dy$$

$$- \int_0^R p_{\text{out}}\left(t^{n+1}\right) \varphi_{x,h}^f|_{x=L} dy - J^n \beta \int_{\Gamma(t^n)} p_h^n \boldsymbol{n}^f \cdot \boldsymbol{\varphi}_h^f d\boldsymbol{x}.$$

Then set $p_h^{n+1} = p_h^{n+2/3}$.

Problem A2(b): We discretize problem A2(b) in time using again the backward Euler method. To solve the resulting advection problem, we use a positivity-preserving ALE finite element scheme, which preserves conservation of mass at the discrete level. Details of the scheme are presented in [63].

4. ENERGY ESTIMATE ASSOCIATED WITH UNCONDITIONAL STABILITY OF THE SCHEME FOR $\beta = 0$

We will show that the proposed operator-splitting scheme satisfies an energy estimate, which is associated with unconditional stability of the scheme for all the parameters in the problem when $\beta = 0$. This will be performed for the basic splitting algorithm, mentioned in Section 3.1.1, where the splitting consists of solving two sub-problems:

A1. An elastodynamics sub-problem for the structure.
A2. A fluid sub-problem, coupled with structure inertia (and the viscous part of the structure equation if $\epsilon \neq 0$).

We will use energy estimates to show that the energy of the discretized problem mimics the energy of the continuous problem. More precisely, we will show that the total energy of the discretized problem plus viscous dissipation of the discretized problem is bounded by the discrete energy of the initial data and the work performed by the inlet and outlet dynamic pressure data. In contrast with similar results appearing in literature [35,37,43,51], which consider simplified models without fluid advection, and linearized fluid–structure coupling calculated at a fixed fluid domain boundary, in this manuscript, we derive the corresponding energy estimate for a full, nonlinear FSI problem, which includes fluid advection, and the coupling is achieved at the moving fluid–structure interface.

To simplify the analysis, the following assumptions that do not influence stability of the scheme will be considered:

1. Only radial displacement of the fluid–structure interface is allowed, that is, $\hat{U}|_{r=R} \cdot \hat{e}_z = 0$ at the fluid–structure interface. The FSI problem with this boundary condition is well defined. This assumption does not affect stability of the scheme related to the added mass effect. In fact, the same assumption was considered in the original work on added mass effect by Causin *et al*. [35]. In the present manuscript, this simplifies the form of the energy estimates in the proof.
2. The problem is driven by the dynamic inlet and outlet pressure data, and the flow enters and leaves the fluid domain parallel to the horizontal axis:

$$p + \frac{\rho_f}{2}|\boldsymbol{v}|^2 = p_{\text{in/out}}(t), \; v_r = 0, \text{ on } \Gamma_{\text{in/out}}.$$

We consider $\beta = 0$ here because, in this case, it is easier to prove the related energy estimates. Our numerical results presented in [38] indicate that only accuracy, not stability, is affected by changing β between 0 and 1. Using energy estimates to prove unconditional stability of the scheme with $\beta \neq 0$ would be significantly more difficult. We mention a related work, however, in which unconditional stability of the kinematically coupled β-scheme for $\beta \in [0, 1]$ was proved for a simplified, linearized FSI problem with a thin structure, using different techniques from those presented here (Čanić *et al*. (2013), unpublished data). In the present paper, for the first time, we derive an energy estimate associated with unconditional stability of the full, nonlinear FSI problem, defined on a moving domain, with nonlinear fluid–structure coupling. The same proof applies to problems where the thick structure is replaced by a thin structure. In that case, the kinematically coupled β-scheme is a fully partitioned scheme [38,40].

We begin by first deriving an energy equality of the continuous, coupled FSI problem.

4.1. The energy of the continuous coupled problem

To formally derive an energy equality of the coupled FSI problem, we multiply the structure equations by the structure velocity, the balance of momentum in the fluid equations by the fluid velocity, and integrate by parts over the respective domains using the incompressibility condition. The dynamic and kinematic coupling conditions are then used to couple the fluid and structure sub-problems. The resulting equation represents the total energy of the problem.

The following identities are used in this calculation:

$$\int_{\Omega^f(t)} \frac{\partial \boldsymbol{v}}{\partial t} \boldsymbol{v} d\boldsymbol{x} = \frac{1}{2}\frac{d}{dt}\int_{\Omega^f(t)} |\boldsymbol{v}|^2 d\boldsymbol{x} - \frac{1}{2}\int_{\Gamma(t)} |\boldsymbol{v}|^2 \boldsymbol{v}\cdot\boldsymbol{n}^f dS, \tag{43}$$

$$\int_{\Omega^f(t)} (\boldsymbol{v}\cdot\nabla)\boldsymbol{v}\cdot\boldsymbol{v} d\boldsymbol{x} = \frac{1}{2}\int_{\partial\Omega^f(t)} |\boldsymbol{v}|^2 \boldsymbol{v}\cdot\boldsymbol{n}^f dS. \tag{44}$$

The first is just the transport theorem. The second one is obtained using integration by parts.

The boundary integral associated with the convective term (44) is simplified as follows. The portion corresponding to Γ_b is zero because of the symmetry boundary condition, which implies $\boldsymbol{v}\cdot\boldsymbol{n} = 0$ on Γ_b. The portion corresponding to $\Gamma(t)$ is canceled with the same term appearing in the transport formula (43). Finally, the boundary terms on $\Gamma_{\text{in/out}}$ are absorbed by the dynamic pressure boundary conditions. The fluid sub-problem implies the following:

$$\frac{1}{2}\frac{d}{dt}\left\{\rho_f||\boldsymbol{v}||^2_{L^2(\Omega^f(t))}\right\} + 2\mu_f||\boldsymbol{D}(\boldsymbol{v})||^2_{L^2(\Omega(t))}$$

$$-\int_0^R p_{\text{in}}(t)v_z|_{z=0}dr + \int_0^R p_{\text{out}}(t)v_z|_{z=L}dr = \int_{\Gamma(t)} \boldsymbol{\sigma}\boldsymbol{n}^f\cdot\boldsymbol{v}\, dS.$$

The integral on the right-hand side can be written in Lagrangian coordinates as

$$\int_{\Gamma(t)} \boldsymbol{\sigma}\boldsymbol{n}^f\cdot\boldsymbol{v}\, dS = \int_{\hat{\Gamma}} \widehat{\boldsymbol{\sigma}\boldsymbol{n}^f}\cdot\hat{\boldsymbol{v}}\, J\, d\hat{z}, \tag{45}$$

where J is the Jacobian of the transformation from the Eulerian to Lagrangian coordinates. We use the kinematic and dynamic lateral boundary conditions (11)–(12) to obtain

$$\int_{\hat{\Gamma}} \widehat{\boldsymbol{\sigma}\boldsymbol{n}^f}\cdot\hat{\boldsymbol{v}}\, J\, d\hat{z} = -\int_{\hat{\Gamma}} \left[\boldsymbol{S}\boldsymbol{n}^s\cdot\frac{\partial\hat{\boldsymbol{U}}}{\partial t} - \epsilon\frac{\partial}{\partial\boldsymbol{n}^s}\left(\frac{\partial\hat{\boldsymbol{U}}}{\partial t}\right)\cdot\frac{\partial\hat{\boldsymbol{U}}}{\partial t}\right]\Bigg|_{\hat{\Gamma}} d\hat{z}. \tag{46}$$

After adding the energy equalities associated with the fluid problem and the thick structure problem, and after using the coupling expressed in (46), one obtains the following energy equality of the coupled FSI problem:

$$\frac{d}{dt}\left\{\underbrace{\frac{\rho_f}{2}||\boldsymbol{v}||^2_{L^2(\Omega^f(t))} + \frac{\rho_s}{2}\left\|\frac{\partial\hat{\boldsymbol{U}}}{\partial t}\right\|^2_{L^2(\hat{\Omega}^s)}}_{\text{Fluid and Structure Kinetic Energy}}\right.$$

$$\left.\underbrace{+\frac{\gamma}{2}||\hat{\boldsymbol{U}}||^2_{L^2(\hat{\Omega}^s)} + \mu_s||\boldsymbol{D}(\hat{\boldsymbol{U}})||^2_{L^2(\hat{\Omega}^s)} + \frac{\lambda_s}{2}||\nabla\cdot\hat{\boldsymbol{U}}||^2_{L^2(\hat{\Omega}^s)}}_{\text{Structure Elastic Energy}}\right\} \tag{47}$$

$$+\underbrace{2\mu_f||\boldsymbol{D}(\boldsymbol{v})||^2_{L^2(\Omega^f(t))}}_{\text{Fluid Viscous Energy}} + \underbrace{\epsilon\left\|\nabla\frac{\partial\hat{\boldsymbol{U}}}{\partial t}\right\|^2_{L^2(\hat{\Omega}^s)}}_{\text{Structure Viscous Energy}}$$

$$= \int_0^R p_{\text{in}}(t)v_z|_{z=0}dr - \int_0^R p_{\text{out}}(t)v_z|_{z=L}dr - \int_{\hat{\Gamma}^s_{ext}} P_{ext}\frac{\partial\hat{U}_r}{\partial t}dS.$$

To obtain energy estimates for the proposed operator-splitting scheme, we first write the main steps of the splitting scheme in weak form. For this purpose, we start by writing the weak form of the problem written in ALE formulation, with dynamics pressure inlet and outlet data, and then split the weak ALE form, following the operator-splitting approach presented in the previous section.

4.2. The weak form of the continuous coupled problem in ALE form

We consider the ALE form of the fluid equations (15)–(16), coupled with the initial and boundary conditions (3)–(12), where the inlet and outlet conditions for the fluid problem are the *dynamic pressure data*. As we shall see later, it is convenient to write the fluid and ALE advection term in symmetric form, giving rise to the following weak formulation: for $t \in (0, T)$, find $\left(v, \hat{U}, p\right) \in V^f(t) \times \hat{V}^s \times Q(t)$ such that $v = \hat{U}_t \circ \mathcal{A}_t^{-1}$ on $\Gamma(t)$, and the following holds:

$$
\begin{aligned}
\rho_f \int_{\Omega^f(t)} &\frac{\partial v}{\partial t}\bigg|_{\hat{x}} \cdot \varphi \, dx + \frac{\rho_f}{2} \int_{\Omega^f(t)} \left(((v - w) \cdot \nabla)v \cdot \varphi - ((v - w) \cdot \nabla)\varphi \cdot v\right) dx \\
&+ \frac{\rho_f}{2} \int_{\Omega^f(t)} (\nabla \cdot w) \, v \cdot \varphi \, dx + 2\mu_f \int_{\Omega^f(t)} D(v) : D(\varphi) dx \\
&- \int_{\Omega^f(t)} p \nabla \cdot \varphi \, dx + \rho_s \int_{\hat{\Omega}^s} \frac{\partial^2 \hat{U}}{\partial t^2} \cdot \hat{\psi} \, dx + 2\mu_s \int_{\hat{\Omega}^s} D(\hat{U}) : D(\hat{\psi}) dx \\
&+ \lambda_s \int_{\hat{\Omega}^s} \left(\nabla \cdot \hat{U}\right) \left(\nabla \cdot \hat{\psi}\right) dx + \gamma \int_{\hat{\Omega}^s} \hat{U} \cdot \hat{\psi} \, dx + \epsilon \int_{\hat{\Omega}^s} \nabla \frac{\partial \hat{U}}{\partial t} : \nabla \hat{\psi} \, dx \\
&+ \int_{\hat{\Gamma}^s_{ext}} P_{ext} \left(\hat{\psi} \cdot n^s_{ext}\right) dS = \int_0^R p_{in}(t)\varphi_z|_{z=0} dr - \int_0^R p_{out}(t)\varphi_z|_{z=L} dr,
\end{aligned}
\tag{48}
$$

and

$$
\int_{\Omega^f(t)} q \nabla \cdot v \, dx = 0,
$$

for all $\left(\varphi, \hat{\psi}, q\right) \in V^{fsi}(t) \times Q(t)$, where $V^{fsi}(t)$ and $Q(t)$ are defined by (17)–(20).

This weak formulation is consistent with the problem. Indeed, integration by parts of one half of the convective term gives

$$
\begin{aligned}
\frac{1}{2} \int_{\Omega^f(t)} ((v - w) \cdot \nabla)v \cdot \varphi = &-\frac{1}{2} \int_{\Omega^f(t)} ((v - w) \cdot \nabla)\varphi \cdot v + \frac{1}{2} \int_{\Omega^f(t)} (\nabla \cdot w)v \cdot \varphi \\
&+ \frac{1}{2} \int_{\partial\Omega^f(t)} ((v - w) \cdot n)v \cdot \varphi.
\end{aligned}
$$

Here, we have used the fact that $\nabla \cdot v = 0$. The last term in this expression, that is, the boundary integral, can be evaluated as follows: on $\Gamma(t)$, we recall that $v = w$ and so that part is zero; on Γ_b, we have $v \cdot n = w \cdot n = 0$, and so this contribution is zero as well; finally, on $\Gamma_{in/out}$, we have $w = 0$, and the remaining quadratic velocity term is exactly the quadratic velocity contribution in dynamic pressure. Therefore, the weak form (48) is consistent with problems (15)–(16) and (3)–(12) in ALE form, with dynamic inlet and outlet pressure data.

4.3. The time discretization via operator splitting in weak form

We perform the time discretization via operator splitting, described in Section 3.1.2, and write each of the split sub-problems in weak form. To simplify the energy estimate proof, we keep the entire fluid sub-problem together, without splitting the advection problem from the time-dependent Stokes problem. The main features of the scheme, which are related to how the fluid and structure problems are separated, are left intact in the stability analysis. Therefore, we split the coupled FSI problem into the following:

A1. An elastodynamics sub-problem for the structure.
A2. A fluid sub-problem, coupled with structure inertia (and the viscous part of the structure equation if $\epsilon \neq 0$).

We discretize the problem in time as described in Section 3.2. As our stability analysis does not depend on the spatial discretization, we leave the spatial operators in continuous form. To write the

weak forms of the structure and fluid sub-problems, we use the bilinear forms defined in (39)–(42). A weak formulation of our semi-discrete operator-splitting numerical scheme is given as follows:

Problem A1. (The structure sub-problem) Find $\hat{U}^{n+1/2} \in \hat{V}^s$ and $\hat{V}^{n+1/2} \in \hat{V}^s$ such that for all $(\hat{\varphi}^s, \phi^s) \in \hat{V}^s \times \hat{V}^s$ and $t \in (t^n, t^{n+1})$:

$$\rho_s \int_{\hat{\Omega}^s} \frac{\hat{V}^{n+1/2} - \hat{V}^n}{\Delta t} \cdot \hat{\varphi}^s \, d\boldsymbol{x} + a_e \left(\frac{\hat{U}^n + \hat{U}^{n+1/2}}{2}, \hat{\varphi}^s \right) = 0,$$

$$\rho_s \int_{\hat{\Omega}^s} \left(\frac{\hat{V}^n + \hat{V}^{n+1/2}}{2} - \frac{\hat{U}^{n+1/2} - \hat{U}^n}{\Delta t} \right) \cdot \phi^s \, d\boldsymbol{x} = 0. \tag{49}$$

In this step, $\partial \boldsymbol{v} / \partial t = 0$, so $\boldsymbol{v}^{n+1/2} = \boldsymbol{v}^n$.

Problem A2. (The fluid sub-problem) Find $\left(\boldsymbol{v}^{n+1}, \hat{\boldsymbol{V}}^{n+1}, p^{n+1} \right) \in V^{fsi}(t) \times Q^f(t)$ such that for all $(\boldsymbol{\varphi}^f, \hat{\boldsymbol{\varphi}}^v, \psi^f) \in V^{fsi}(t) \times Q^f(t)$ and $t \in (t^n, t^{n+1})$:

$$\rho_f \int_{\Omega^f(t^n)} \frac{\boldsymbol{v}^{n+1} - \boldsymbol{v}^{n+1/2}}{\Delta t} \cdot \boldsymbol{\varphi}^f \, d\boldsymbol{x} + \frac{\rho_f}{2} \int_{\Omega^f(t^n)} \left(\nabla \cdot \boldsymbol{w}^{n+\frac{1}{2}} \right) \boldsymbol{v}^{n+1} \boldsymbol{\varphi}^f$$

$$+ \frac{\rho_f}{2} \int_{\Omega^f(t^n)} \left(\left(\boldsymbol{v}^n - \boldsymbol{w}^{n+1/2} \right) \cdot \nabla \right) \boldsymbol{v}^{n+1} \cdot \boldsymbol{\varphi}^f - \left(\left(\boldsymbol{v}^n - \boldsymbol{w}^{n+1/2} \right) \cdot \nabla \right) \boldsymbol{\varphi}^f \cdot \boldsymbol{v}_n^{n+1} \right)$$

$$+ a_f \left(\boldsymbol{v}^{n+1}, \boldsymbol{\varphi}^f \right) - b_f \left(p^{n+1}, \boldsymbol{\varphi}^f \right) + \rho_s \int_{\hat{\Omega}^s} \frac{\hat{\boldsymbol{V}}^{n+1} - \hat{\boldsymbol{V}}^{n+1/2}}{\Delta t} \cdot \hat{\boldsymbol{\varphi}}^v \, d\boldsymbol{x} + a_v \left(\hat{\boldsymbol{V}}^{n+1}, \hat{\boldsymbol{\varphi}}^v \right)$$

$$= \int_0^R p_{\text{in}} \left(t^{n+1} \right) \varphi_x^f |_{x=0} dy - \int_0^R p_{\text{out}} \left(t^{n+1} \right) \varphi_x^f |_{x=L} dy, \tag{50}$$

$$b_f \left(\psi^f, \boldsymbol{v}^{n+1} \right) = 0.$$

In this step, $\partial \hat{U} / \partial t = 0$, so $\hat{U}^{n+1} = \hat{U}^{n+1/2}$.

Notice that in problem A2, we have taken the ALE velocity $\boldsymbol{w}^{n+1/2}$ from the just-calculated problem A1, and not from the previous time step. As in problem A2, the fluid domain does not change, $\boldsymbol{w}^{n+1/2} = \boldsymbol{w}^{n+1}$. This is important in proving energy estimates that are associated with the stability of the splitting scheme for the full, nonlinear FSI problem defined on the moving domain. Namely as we shall see later, by using this ALE velocity, we will be able to approximate the total discrete energy at t^{n+1}, which includes the kinetic energy due to the motion of the fluid domain at t^{n+1}, described by $\boldsymbol{w}^{n+1}$.

4.4. Energy estimate associated with unconditional stability of the splitting scheme

Let $\mathcal{E}_f^n$ denote the discrete energy associated with (50), and let $\mathcal{E}_s^n$ denote the discrete energy associated with (49) at time level $n\Delta t$:

$$\mathcal{E}_f^n := \frac{\rho_f}{2} ||\boldsymbol{v}^n||_{L^2(\Omega^f(t^n))}^2, \tag{51}$$

$$\mathcal{E}_s^n := \frac{\rho_s}{2} ||\hat{\boldsymbol{V}}^n||_{L^2(\hat{\Omega}^s)}^2 + \mu_s ||D\left(\hat{\boldsymbol{U}}^n\right)||_{L^2(\hat{\Omega}^s)}^2 + \frac{\lambda_s}{2} ||\nabla \cdot \hat{\boldsymbol{U}}^n||_{L^2(\hat{\Omega}^s)}^2$$

$$+ \frac{\gamma}{2} ||\hat{\boldsymbol{U}}^n||_{L^2(\hat{\Omega}^s)}^2. \tag{52}$$

The following energy estimate holds for the full nonlinear FSI problem, satisfying the aforementioned assumptions 1 and 2.

Theorem 1 (Energy estimate of the operator-splitting scheme)
Let $\left\{ \left(v^n, \hat{V}^n, \hat{U}^n \right) \right\}_{0 \leqslant n \leqslant N}$ be a solution of (49)–(50). Then at any time level $\tilde{n}\Delta t$, where $0 \leqslant \tilde{n} \leqslant N$, the following energy estimate holds:

$$
\mathcal{E}_f^{\tilde{n}} + \mathcal{E}_s^{\tilde{n}} + \frac{\rho_f}{2} \sum_{n=0}^{\tilde{n}-1} ||v^{n+1} - v^n||_{L^2(\Omega^f(t^n))}^2 + \frac{\rho_s}{2} \sum_{n=0}^{\tilde{n}-1} ||\hat{V}^{n+1} - \hat{V}^{n+1/2}||_{L^2(\Omega^s)}^2
$$

$$
+ \mu_f \Delta t \sum_{n=0}^{\tilde{n}-1} ||D\left(v^{n+1}\right)||_{L^2(\Omega^f(t^n))}^2 + \epsilon \Delta t \sum_{n=0}^{\tilde{n}-1} ||\nabla \hat{V}^{n+1}||_{L^2(\hat{\Omega}^s)}^2 \tag{53}
$$

$$
\leqslant \mathcal{E}_f^0 + \mathcal{E}_s^0 + \frac{C\Delta t}{2\mu_f} \sum_{n=0}^{\tilde{n}-1} ||p_{\text{in}}(t^n)||_{L^2(0,R)}^2 + \frac{C\Delta t}{2\mu_f} \sum_{n=0}^{\tilde{n}-1} ||p_{\text{out}}(t^n)||_{L^2(0,R)}^2.
$$

The first line in the energy estimate corresponds to the kinetic energy of the fluid and the total energy of the structure, while the second line describes viscous dissipation in the fluid and the structure. They are estimated by the initial kinetic energy of the fluid, by the total initial energy of the structure, and by the work performed by the inlet and outlet pressure data.

Proof
To prove the energy estimate, we test the structure problem (49) with

$$
\left(\hat{\varphi}^s, \hat{\phi}^s \right) = \left(\frac{\hat{U}^{n+1/2} - \hat{U}^n}{\Delta t}, \frac{\hat{V}^{n+1/2} - \hat{V}^n}{\Delta t} \right),
$$

and problem (50) with

$$
\left(\varphi^f, \hat{\varphi}^v, \psi^f \right) = \left(v^{n+1}, \hat{V}^{n+1}, p^{n+1} \right).
$$

As we have assumed that the fluid–structure interface deforms only in the radial direction, that is, $\hat{U}|_{r=R} = \hat{U}|_{r=R}\hat{e}_r$, we can explicitly calculate the ALE mapping at every step and, more importantly, calculate the associated ALE velocity w. For this purpose, we denote by η the radial displacement of the fluid–structure interface, namely

$$
\hat{\eta} := \hat{U}|_{\hat{r}=R}\hat{e}_r, \text{ and } \hat{\eta}^n := \hat{U}\left(\hat{z}, t^n \right)|_{\hat{r}=R}\hat{e}_r.
$$

We consider the following simple ALE mapping:

$$
A_{t^n} : \hat{\Omega}^f \to \Omega^f(t^n), \quad A_{t^n}(\hat{z}, \hat{r}) := \left(\hat{z}, \frac{R + \hat{\eta}^n}{R}\hat{r} \right)^{\tau}.
$$

We will also need the explicit form of the ALE mapping from the computational domain $\Omega^f(t^n)$ to $\Omega^f(t^{n+1})$, which is given by

$$
A_{t^{n+1}} \circ A_{t^n}^{-1} : \Omega^f(t^n) \to \Omega^f\left(t^{n+1} \right), \quad A_{t^{n+1}} \circ A_{t^n}^{-1}(z, r) = \left(z, \frac{R + \hat{\eta}^{n+1}}{R + \hat{\eta}^n}r \right)^{\tau}.
$$

The corresponding Jacobian and the ALE velocity are given by

$$
J_n^{n+1} := \frac{R + \hat{\eta}^{n+1}}{R + \hat{\eta}^n}, \quad w^{n+1} = \frac{1}{\Delta t}\frac{\hat{\eta}^{n+1} - \hat{\eta}^n}{R + \hat{\eta}^n} r\hat{e}_r. \tag{54}
$$

In problem A1 where we just calculated the updated location of the structure, $\hat{\eta}^n$ determines the 'reference domain', and $\hat{\eta}^{n+1/2}$, which is the same as $\hat{\eta}^{n+1}$, determines the location of the

new domain. Therefore, the time derivative of the interface displacement is approximated by $\left(\hat{\eta}^{n+1} - \hat{\eta}^n\right)/\Delta t$, which enters the expression for the ALE velocity $\boldsymbol{w}^{n+1}$. Again, notice that $\boldsymbol{w}^{n+1/2} = \boldsymbol{w}^{n+1}$.

We begin by considering the fluid sub-problem and the advection terms involving the fluid and ALE advection. After replacing the test functions by the fluid velocity at time $n + 1$, we first notice that the symmetrized advection terms cancel out. What is left are the terms

$$\rho_f \int_{\Omega^f(t^n)} \frac{\boldsymbol{v}^{n+1} - \boldsymbol{v}^n}{\Delta t} \boldsymbol{v}^{n+1} + \frac{\rho_f}{2} \int_{\Omega^f(t^n)} \left(\nabla \cdot \boldsymbol{w}^{n+\frac{1}{2}}\right) |\boldsymbol{v}^{n+1}|^2.$$

To deal with the term on the left, we use the following identity:

$$a(a - b) = \frac{1}{2}\left(a^2 - b^2 + (a - b)^2\right). \tag{55}$$

To deal with the term on the right-hand side, we use the expression for $\boldsymbol{w}^{n+1/2}$, given by (54), where we recall that $\boldsymbol{w}^{n+1/2} = \boldsymbol{w}^{n+1}$, as in the second step, the structure location does not change. We obtain

$$\frac{\rho_f}{2} \frac{1}{\Delta t} \int_{\Omega^f(t^n)} \left(1 + \frac{\hat{\eta}^{n+1} - \hat{\eta}^n}{R + \hat{\eta}^n}\right) |\boldsymbol{v}^{n+1}|^2 + |\boldsymbol{v}^{n+1} - \boldsymbol{v}^n|^2 - |\boldsymbol{v}^n|^2$$

$$= \frac{\rho_f}{2} \frac{1}{\Delta t} \int_{\Omega^f(t^n)} \left(\frac{R + \hat{\eta}^{n+1}}{R + \hat{\eta}^n} |\boldsymbol{v}^{n+1}|^2 + |\boldsymbol{v}^{n+1} - \boldsymbol{v}^n|^2 - |\boldsymbol{v}^n|^2\right).$$

Now notice that $\left(R + \hat{\eta}^{n+1}\right)/\left(R + \hat{\eta}^n\right)$ is exactly the Jacobian of the ALE mapping from $\Omega^f(t^n)$ to $\Omega^f(t^{n+1})$; see (54); and so we can convert that integral into an integral over $\Omega^f\left(t^{n+1}\right)$ to recover the kinetic energy of the fluid at the next time step:

$$\frac{\rho_f}{2} \frac{1}{\Delta t} \int_{\Omega^f(t^n)} \frac{R + \hat{\eta}^{n+1}}{R + \hat{\eta}^n} |\boldsymbol{v}^{n+1}|^2 = \frac{\rho_f}{2} \frac{1}{\Delta t} \int_{\Omega^f\left(t^{n+1}\right)} |\boldsymbol{v}^{n+1}|^2.$$

This calculation effectively shows that the kinetic energy of the fluid at the next time step accounts for the kinetic energy of the fluid at the previous time step, plus the kinetic energy due to the motion of the fluid domain. Therefore, even at the discrete level, we see that the energy of the discretized problem mimics well the energy of the continuous problem.

Notice that this calculation also shows that the ALE mapping and its Jacobian satisfy the geometric conservation law; see [64] for more details. A similar result was shown in [65] for the ALE mapping, which is the harmonic extension of the boundary to the entire domain.

To deal with the structure sub-problem, we do not have the same problem associated with moving domains, as the structure problem is defined in Lagrangian coordinates, namely on a fixed domain $\hat{\Omega}^s$. We use formula (55) to calculate the kinetic energy of the structure at the next time step, in terms of the kinetic energy of the structure at the previous time step, plus a quadratic term $||\hat{V}^{n+1} - \hat{V}^{n+1/2}||^2_{L^2\left(\hat{\Omega}^s\right)}$ that accounts for the kinetic energy due to the difference in the velocities of the structure between the two time steps.

Finally, we add the corresponding energy equalities for the fluid and structure sub-problems. We obtain

$$\mathcal{E}_f^{n+1} + \mathcal{E}_s^{n+1} + \frac{\rho_f}{2}||\boldsymbol{v}^{n+1} - \boldsymbol{v}^n||^2_{L^2(\Omega^f(t^n))} + \frac{\rho_s}{2}||\hat{V}^{n+1} - \hat{V}^{n+1/2}||^2_{L^2\left(\hat{\Omega}^s\right)}$$

$$+ 2\mu_f \Delta t ||D\left(\boldsymbol{v}^{n+1}\right)||^2_{L^2(\Omega^f(t^n))} + \epsilon \Delta t \sum_{n=0}^{\tilde{n}-1} ||\nabla \hat{V}^{n+1}||^2_{L^2\left(\hat{\Omega}^s\right)}$$

$$= \mathcal{E}_f^n + \mathcal{E}_s^n + \Delta t \int_0^R p_{\text{in}}\left(t^{n+1}\right) \boldsymbol{v}^{n+1}|_{x=0} dy - \Delta t \int_0^R p_{\text{out}}\left(t^{n+1}\right) \boldsymbol{v}^{n+1}|_{x=L} dy.$$

To bound the right-hand side of this equality, we use the Cauchy–Schwartz and Young's inequalities, to obtain

$$\Delta t \int_0^R p_{\text{in}} \left(t^{n+1}\right) \boldsymbol{v}^{n+1}|_{x=0} dy - \Delta t \int_0^R p_{\text{out}} \left(t^{n+1}\right) \boldsymbol{v}^{n+1}|_{x=L} dy$$

$$\leqslant \frac{\Delta t}{2\epsilon_1} ||p_{\text{in}}(t^n)||^2_{L^2(0,R)} + \frac{\Delta t}{2\epsilon_1} ||p_{\text{out}}(t^n)||^2_{L^2(0,R)} + \epsilon_1 \Delta t ||\boldsymbol{v}^{n+1}||^2_{L^2(0,R)}.$$

From the trace and Korn inequalities, we have

$$\Delta t \int_0^R p_{\text{in}} \left(t^{n+1}\right) \boldsymbol{v}^{n+1}|_{x=0} dy - \Delta t \int_0^R p_{\text{out}} \left(t^{n+1}\right) \boldsymbol{v}^{n+1}|_{x=L} dy$$

$$\leqslant \frac{\Delta t}{2\epsilon_1} ||p_{\text{in}}(t^n)||^2_{L^2(0,R)} + \frac{\Delta t}{2\epsilon_1} ||p_{\text{out}}(t^n)||^2_{L^2(0,R)} + \epsilon_1 C \Delta t ||\boldsymbol{D}\left(\boldsymbol{v}^{n+1}\right)||^2_{L^2(\Omega^f(t^n))},$$

where C is the constant from the trace and Korn inequalities. In general, Korn's constant depends on the domain. It was shown, however, that for domains associated with FSI problems of the type studied in this manuscript, the Korn's constant is independent of the sequence of approximating domains [53, 66].

By setting $\epsilon_1 = \dfrac{\mu_f}{C}$, the last term can be combined with the term on the left-hand side, associated with fluid diffusion. Therefore, so far, we have shown that the following inequality holds:

$$\mathcal{E}_f^{n+1} + \mathcal{E}_s^{n+1} + \frac{\rho_f}{2} ||\boldsymbol{v}^{n+1} - \boldsymbol{v}^n||^2_{L^2(\Omega^f(t^n))} + \frac{\rho_s}{2} ||\hat{V}^{n+1} - \hat{V}^{n+1/2}||^2_{L^2(\hat{\Omega}^s)}$$

$$+ \mu_f \Delta t ||D\left(\boldsymbol{v}^{n+1}\right)||^2_{L^2(\Omega^f(t^n))} + \epsilon \Delta t \sum_{n=0}^{\tilde{n}-1} ||\nabla \hat{V}^{n+1}||^2_{L^2(\hat{\Omega}^s)}$$

$$\leqslant \mathcal{E}_f^n + \mathcal{E}_s^n + \frac{C}{\mu_f} \Delta t ||p_{\text{in}}(t^n)||^2_{L^2(0,R)} + \frac{C}{\mu_f} \Delta t ||p_{\text{out}}(t^n)||^2_{L^2(0,R)}.$$

To obtain an energy estimate for an arbitrary time level $\tilde{n}\Delta t$, where $1 \leqslant \tilde{n} \leqslant N$, in terms of the energy of the initial data, and the work performed by the inlet and outlet dynamic pressure data, we sum the preceding inequalities for $n = 1, \ldots, \tilde{n}$, cancel the corresponding kinetic energy terms appearing on both sides, and obtain the energy estimate (53). □

5. NUMERICAL RESULTS

We consider two test problems. The first was considered in [51] to test performance of a partitioned scheme based on Nitsche's method, with a time penalty term needed for stabilization. The problem involves solving a time-dependent Stokes problem coupled with the equations of linear elasticity, where the coupling is assumed at a fixed fluid domain boundary (linear coupling). The second problem we consider was proposed in [67] and used in [68] as a benchmark problem for FSI with thick elastic walls to test performance of monolithic FSI schemes. In this problem, the full FSI problem (26)–(38) is solved, and the coupling is evaluated at the moving fluid–structure interface (nonlinear coupling). In both examples, the flow is driven by the time-dependent pressure data. To resemble the regime in which instabilities may occur, the fluid and structure densities are taken to be comparable.

We used our operator-splitting scheme with $\beta = 1$ to simulate solutions to the two problems. Our numerical investigations indicate that an increase in $\beta \in [0, 1]$ increases the accuracy of the scheme. A similar experience was also reported in [38] for an FSI problem involving a thin elastic structure. This is why all the simulations presented here correspond to $\beta = 1$.

The value of the viscous parameter ϵ was taken to be zero in both examples. Taking $\epsilon > 0$ regularizes solutions of the FSI problem. Therefore, $\epsilon = 0$ is the most difficult case to consider, as the structure problem in that case is hyperbolic, exhibiting wave phenomena in the structure at disparate time scales from the fluid.

Table I. Parameter values for Example 1.

Parameters	Values	Parameters	Values
Radius R (cm)	0.5	Length L (cm)	5
Fluid density ρ_f (g/cm^3)	1.1	Dyn. viscosity μ (poise)	0.035
Wall density ρ_s (g/cm^3)	1.2	Wall thickness h (cm)	0.1
Lamé coeff. μ_s (dyne/cm^2)	5.75×10^5	Lamé coeff. λ_s (dyne/cm^2)	1.7×10^6
Spring coeff. γ (dyne/cm^4)	0	Viscoel. coeff. ϵ (dyne s/cm^2)	0

In both examples, the results obtained using the proposed operator-splitting scheme are compared with solutions obtained using a monolithic scheme, showing excellent agreement. In the second example, which considers the full FSI problem (26)–(38), we additionally show that our numerical results indicate first-order accuracy in time of the proposed numerical scheme. Finally, we show that the condition number of the fluid sub-problem (problem A2) in the proposed operator-splitting scheme is by several orders of magnitude smaller than the condition number of monolithic schemes because no wave phenomena associated with structural elastodynamics are solved in problem A2 of the scheme.

5.1. Example 1

We consider a simplified FSI problem in which the fluid is modeled by the time-dependent Stokes problem and the structure by the equations of linear elasticity. The fluid–structure coupling is linear in the sense that the fluid domain does not change in time. The flow is driven by the inlet time-dependent pressure data, which are a step function in time:

$$p_{in}(t) = \begin{cases} 10^4 \text{ dyne/cm}^2 & \text{if } t \leq 0.005 \\ 0 & \text{if } t > 0.005 \end{cases}, \quad p_{out}(t) = 0 \; \forall t \in (0, T).$$

The outlet normal stress is kept at zero.

The values of the parameters that determine the fluid and structure geometry, as well as their physical properties, are given in Table I

This problem was suggested in [51] as a test problem to study performance of an explicit scheme for FSI problems, which was based on Nitsche's method. To deal with the instabilities associated with the added mass effect in [51], a weakly consistent stabilization term was added that corresponds to the pressure variations at the interface. This decreased the temporal accuracy of the scheme, which was then corrected by adding certain defect-correction sub-iterations. In [51], this stabilized explicit scheme was solved using the Taylor–Hood ($\mathbb{P}_2/\mathbb{P}_1$) finite elements for the fluid and $\mathbb{P}_1$ elements for the structure. The size of the computational mesh was $h_v = 0.1$. Their simulations were compared with the solution obtained using a monolithic scheme. The time step for the monolithic scheme was $\Delta t = 10^{-4}$, while the time step used in the stabilized explicit scheme based on Nitsche's method was $\Delta t = 10^{-5}$.

In our simulations, we discretize the problem in space by using a finite element approach with an isoparametric version of the Bercovier–Pironneau element spaces, also known as the $\mathbb{P}_1$-iso-$\mathbb{P}_2$ approximation. In this approach, a coarse mesh is used for the pressure (mesh size h_p) and a fine mesh for velocity (mesh size $h_v = h_p/2$). To solve the structure problem, we used $\mathbb{P}_1$ elements on a conforming mesh. To capture all the physically relevant phenomena, in this example, we chose the space discretization step to be $h_v = \frac{1}{\sqrt{Re}} = 0.032$, where Re is the Reynolds number associated with this problem. To achieve comparable accuracy to the scheme proposed in [51], we only needed to take the time step $\Delta t = 10^{-4}$, which was the time step used in [51] for the monolithic solver but not for the stabilized explicit scheme proposed there.

A comparison between the results of the stabilized explicit scheme proposed in [51], the monolithic scheme used in [51], and our operator-splitting scheme is shown in Figure 3. In this figure, the displacement of the fluid–structure interface at the mid-point of the spatial domain was calculated. Excellent agreement was achieved between our method and the corresponding monolithic method,
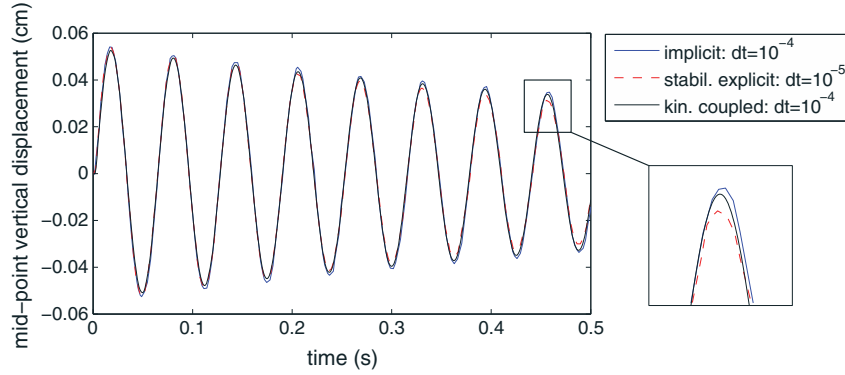
Figure 3. Mid-point vertical displacement computed using a monolithic scheme (blue sold line) with $\Delta t = 10^{-4}$, a stabilized explicit scheme proposed by Burman and Fernandez [51] with $\Delta t = 10^{-5}$ (red dashed line), and the operator-splitting scheme with $\beta = 1$ and $\Delta t = 10^{-4}$ (black solid line).
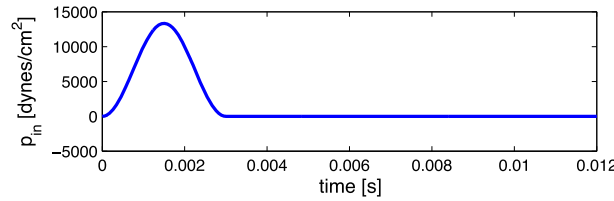

Figure 4. The inlet pressure pulse for Example 2. The outlet normal stress is kept at 0.

Table II. Parameter values for Example 2.

Parameters	Values	Parameters	Values
Radius R (cm)	0.5	Length L (cm)	6
Fluid density ρ_f (g/cm^3)	1	Dyn. viscosity μ (g/cm s)	0.035
Wall density ρ_s (g/cm^3)	1.1	Wall thickness h (cm)	0.1
Lamé coeff. μ_s (dyne/cm^2)	5.75×10^5	Lamé coeff. λ_s (dyne/cm^2)	1.7×10^6
Spring coeff. γ (dyne/cm^4)	4×10^6	Viscoel. coeff. ϵ (dyne s/cm^2)	0

where the time step we used was the same as the time step used in the monolithic solver. In contrast with the stabilized explicit scheme proposed in [51], the operator-splitting scheme proposed in this manuscript does not require stabilization, providing results of this problem that compare well with the results of the monolithic scheme using the same time step as in the monolithic solver.

5.2. Example 2

We consider the fully nonlinear FSI problem (26)–(38) with the fluid–structure coupling evaluated at the moving interface (nonlinear coupling). The flow is driven by the inlet time-dependent pressure data, which is a cosine pulse lasting for $t_{max} = 0.003$ s, while the outlet normal stress is kept at zero:

$$p_{in}(t) = \begin{cases} \frac{p_{max}}{2}\left[1 - \cos\left(\frac{2\pi t}{t_{max}}\right)\right] & \text{if } t \leqslant t_{max} \\ 0 & \text{if } t > t_{max} \end{cases} , \quad p_{out}(t) = 0 \ \forall t \in (0, T),$$

where $p_{max} = 1.333 \times 10^4$ (dyne/cm^2) and $t_{max} = 0.003$ (s). See Figure 4.

This problem was proposed in [67] and used in [68] as a benchmark problem for FSI problems in hemodynamics, involving thick elastic walls.

The domain geometry and the values of all the fluid and structure parameters in this example are given in Table II.

Problem (26)–(38) was solved over the time interval $[0, 0.012]$ s. This is the time it takes the pressure pulse generated at the inlet to travel across the entire fluid domain and reach the outlet.

We solved this problem using the following five different time steps: $\Delta t = 10^{-4}, 5 \times 10^{-5}, 10^{-5}, 5 \times 10^{-6},$ and 10^{-6}. These time steps were used to numerically show that the method is convergent and that its accuracy in time is first order.

As before, to discretize the problem in space, we used the Bercovier–Pironneau element spaces, also known as the $\mathbb{P}_1$-iso-$\mathbb{P}_2$ approximation, with the velocity mesh of size $h_v = 0.01$ and the pressure mesh of size $h_p = 2h_v = 0.02$. To solve the structure problem, the $\mathbb{P}_1$ elements were used on a conforming mesh.

Figures 5 and 6 show 2D plots of the fluid pressure and structure displacement, respectively. The pressure wave, shown in Figure 5, travels from left to right, displacing the thick structure. The colors of the thick structure displacement in Figure 5 denote the magnitude of the radial component of displacement. Figure 6 shows separate snapshots of the longitudinal and radial components of the
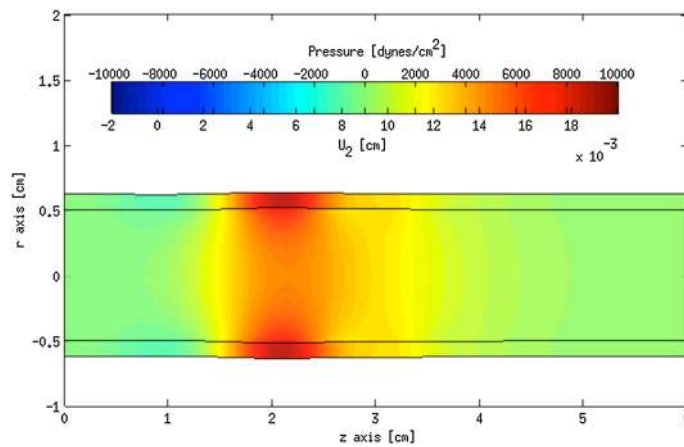
Figure 5. A snapshot of the pressure wave traveling from left to right coupled with the radial component of the structure displacement. The legend shows the values for the pressure (top scale) and displacement (bottom scale) over the same color scale.
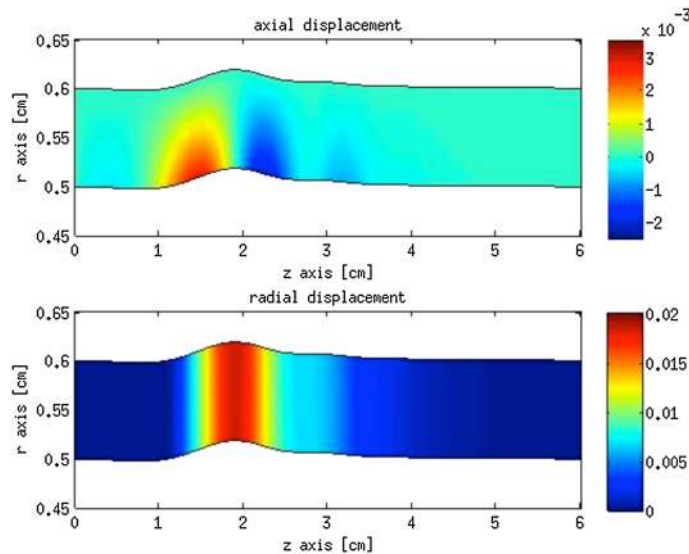

Figure 6. The longitudinal (top) and radial (bottom) components of the structure displacement. Notice how red and blue in longitudinal displacement denote longitudinal stretching of the structure in opposite $(+/-)$ directions.
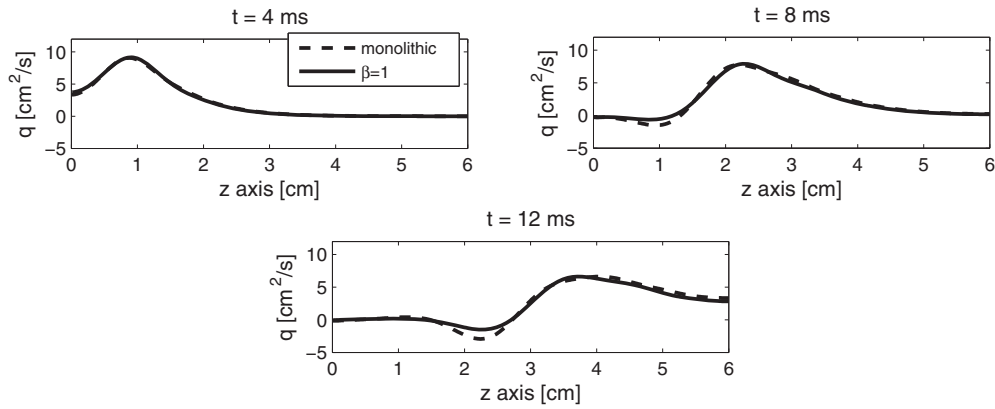
Figure 7. Flow rate versus z, at $t = 4, 8, 12$ ms, computed with the monolithic scheme by Quaini [67] (time step $\Delta t = 10^{-4}$; dashed line) and with our operator-splitting scheme with $\beta = 1$ (time step $\Delta t = 5 \times 10^{-5}$; solid line).
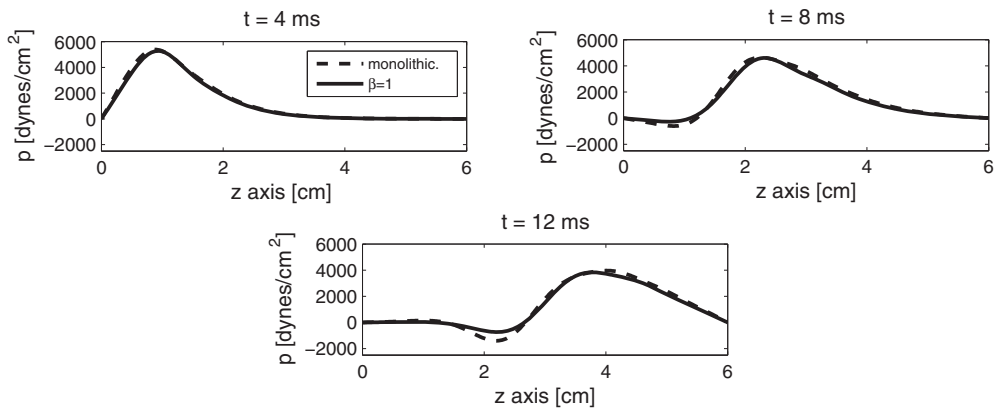

Figure 8. Mean pressure versus z, at $t = 4, 8, 12$ ms, computed with the monolithic scheme by Quaini [67] (time step $\Delta t = 10^{-4}$; dashed line) and with our operator-splitting scheme with $\beta = 1$ (time step $\Delta t = 5 \times 10^{-5}$; solid line).

displacement. Notice how red and blue in longitudinal displacement denote longitudinal stretching of the structure in opposite directions.

The numerical results obtained using the operator-splitting scheme proposed in this manuscript were compared with the numerical results obtained using the monolithic scheme proposed in [67, 68]. The monolithic scheme was solved on the same mesh using stabilized $\mathbb{P}_1$–$\mathbb{P}_1$ elements for the fluid problem and $\mathbb{P}_1$ elements for the structure problem.

Figures 7–9 show the calculated flow rate, mean pressure, and fluid–structure interface displacement, respectively, as functions of the horizontal axis z, for three different snapshots. The three figures show a comparison between our operator-splitting scheme, shown in solid line, and the monolithic scheme of [67, 68], shown in dashed line. In these figures, the time step used in the monolithic scheme was $\Delta t = 10^{-4}$. To obtain roughly the same accuracy, we used the time step $\Delta t / 2 = 5 \times 10^{-5}$. Figures 7–9 show a good comparison between the two solutions.

5.2.1. Convergence in time. In this example, we also study convergence in time of our operator-splitting scheme. For this purpose, we define the reference solution to be the one obtained with $\Delta t = 10^{-6}$. We calculated the relative L^2-errors for the velocity, pressure, and displacement, between the reference solution and the solutions obtained using $\Delta t = 10^{-4}, 5 \times 10^{-5}, 10^{-5}$, and 5×10^{-6}. Figure 10 shows the log–log plot of the relative errors, superimposed over a line with
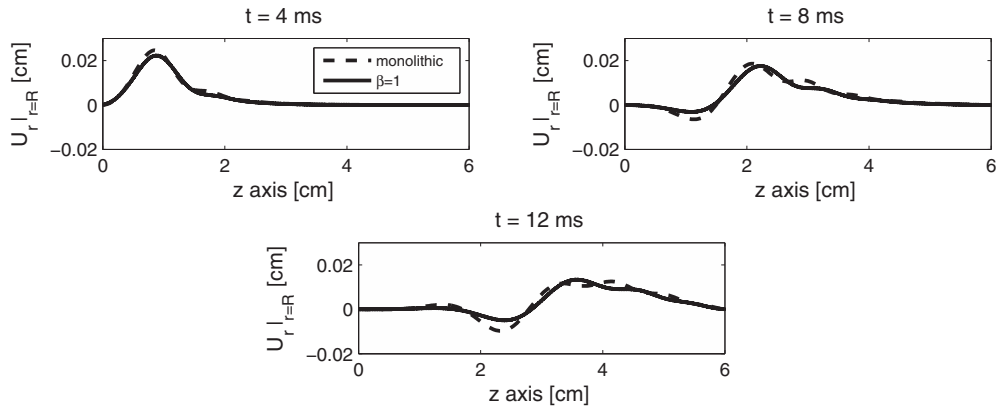
Figure 9. Fluid–structure interface displacement versus z, at $t = 4, 8, 12$ ms, computed with the monolithic scheme by Quaini [67] (time step $\Delta t = 10^{-4}$; dashed line) and with our operator-splitting scheme with $\beta = 1$ (time step $\Delta t = 5 \times 10^{-5}$; solid line).
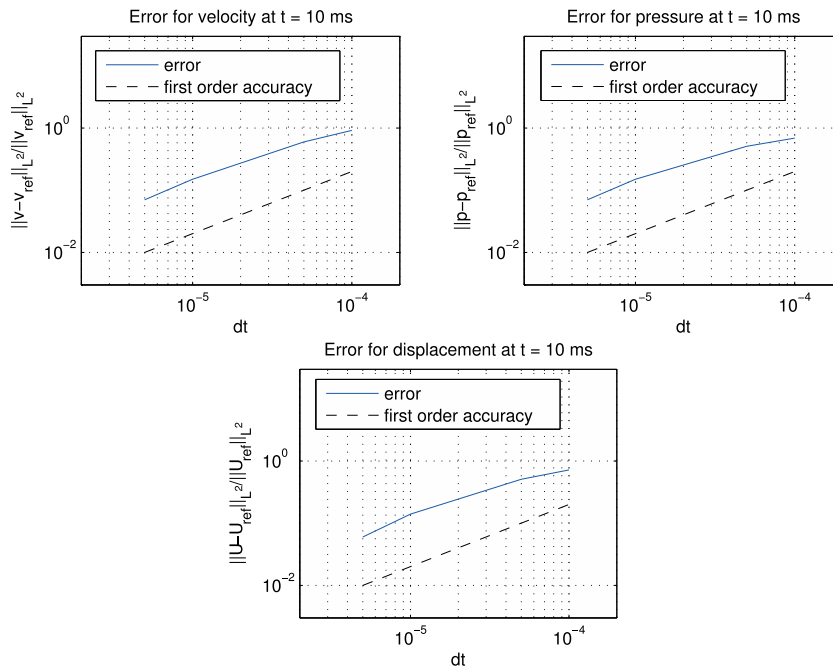

Figure 10. Example 1: figures show relative errors obtained at $t = 10$ ms. Top left: relative error for fluid velocity. Top right: relative error for fluid pressure. Bottom: relative error for the structure displacement.

slope 1, corresponding to first-order accuracy. The slopes indicate that our scheme is first-order accurate in time. Indeed, Table III shows the precise numbers from Figure 10, calculated at time $t = 10$ ms, indicating first order in time convergence for the velocity, pressure, and displacement.

5.2.2. The condition number of the fluid sub-problem in problem A2. We recall that in problem A2 of this operator-splitting scheme, a fluid sub-problem is solved in such a way to include the structure inertia into the fluid sub-problem. This was performed for stability reasons, that is, to avoid issues related to the added mass effect, associated with classical Dirichlet–Neumann partitioned schemes for FSI in hemodynamics. As mentioned earlier, for FSI problems containing a thin fluid–structure interface with mass, including the fluid–structure interface inertia into the fluid sub-problem can be easily accomplished via a Robin-type boundary condition for the fluid sub-problem, leading to a

Table III. Convergence in time calculated at $t = 10$ ms.

Δt	$\frac{\|p-p_{ref}\|_{L^2}}{\|p_{ref}\|_{L^2}}$	L^2 order	$\frac{\|u-u_{ref}\|_{L^2}}{\|u_{ref}\|_{L^2}}$	L^2 order	$\frac{\|U-U_{ref}\|_{L^2}}{\|U_{ref}\|_{L^2}}$	L^2 order
10^{-4}	0.69	—	0.92	—	0.72	—
5×10^{-5}	0.51	0.43	0.60	0.60	0.51	0.5
10^{-5}	0.15	0.76	0.15	0.85	0.14	0.8
5×10^{-6}	0.07	1.06	0.07	1.1	0.06	1.1

fully partitioned scheme [38,53]. In our problem, however, the fluid–structure interface is just a trace of the thick structure in contact with the fluid. In this case, the trace of the fluid–structure interface does not have a well-defined inertia, and we need to include the inertia of the entire thick structure into the fluid sub-problem. As we saw earlier, this is performed by solving a fluid sub-problem together with a simple problem for the structure that takes only the structure inertia into account (and possibly the viscous effects of the structure if $\epsilon \neq 0$). Thus, in problem A2, we solve a simplified coupled problem consisting of a fluid sub-problem, and a structure sub-problem involving only structure inertia, coupled through a simple continuity of stresses condition. Even though this is reminiscent of monolithic schemes, we show here that the condition number of this fluid sub-problem is by several orders of magnitude smaller than the condition number of the monolithic scheme by Quaini [67,68]. Indeed, we calculated the condition number κ of the stiffness matrix in problem A2 of our operator-splitting scheme and obtained that $\kappa_{split} = 1.08 \times 10^4$. Similarly, we calculated the related condition number for the stiffness matrix of the monolithic scheme by Quaini [67,68] and obtained that it equals $\kappa_{mono} = 7.82 \times 10^8$. This is directly related to the fact that in problem A2 of our scheme, no structural elastodynamics problem was solved that would capture the wave phenomena in the structure traveling at disparate time scales from the pressure wave in the fluid.

Therefore, although the problem in problem A2 is solved on both fluid and structure domains, its condition number is equivalent to that of pure fluid solvers. Thus, the proposed operator-splitting scheme consists of a fluid module and a structure module, which can be easily replaced if different structure models or different solvers are to be used; see, for example, [54]. Furthermore, for more general multi-physics problems, additional modules can be easily added to capture different physics in the problem, as was performed in (Bukač *et al.* (2013), unpublished data) to study FSI with multi-layered structures, in (Bukač *et al.* (2013), unpublished data) to study FSI with multi-layered poroelastic walls, or in (Muha and Čanić (2013), unpublished data) to include a model of a stent in the underlying FSI problem. Modularity, unconditional stability, and simple implementation are the features that make this operator-splitting scheme particularly appealing for multi-physics problems involving FSI.

6. CONCLUSIONS

This work proposes a modular scheme for FSI problems with thick structures. The proposed scheme is based on the Lie operator-splitting approach, which separates the fluid from the structure sub-problem, and on using an ALE approach to deal with the motion of the fluid domain. To achieve unconditional stability without sub-iterations in each time step, the fluid sub-problem includes structure inertia, which requires solving the fluid sub-problem on both domains, that is, the fluid and structure domains. While this is reminiscent of monolithic schemes, the condition number of the fluid sub-step is significantly smaller than the condition number associated with classical FSI monolithic schemes. This is because the wave propagation in the elastic structure is treated separately in the structure sub-problem and not together with the fluid problem, as in classical monolithic schemes. The advantage of this approach over classical monolithic schemes is the possibility to use larger time steps, the separation of dissipative versus non-dissipative features of the coupled problem allowing the use of non-dissipative solvers to treat wave propagation in the structure, and modularity, which allows simple extensions of the scheme to capture different multi-physics problems associated with FSI. A disadvantage of this scheme over classical partitioned schemes is that the

fluid sub-step requires solving the associated problem on both the fluid and structure domains in a monolithic fashion. However, unlike the classical Dirichlet–Neumann partitioned schemes, the proposed scheme is unconditionally stable for all the parameters in the problem. This was shown in the present manuscript by proving an energy estimate associated with unconditional stability of the scheme, for the full, nonlinear FSI problem.

REFERENCES

1. Peskin CS. Numerical analysis of blood flow in the heart. *Journal of Computational Physics* 1977; **25**(3):220–252.
2. Peskin CS, McQueen DM. Modeling prosthetic heart valves for numerical analysis of blood flow in the heart. *Journal of Computational Physics* 1980; **37**(1):113–132.
3. Fauci LJ, Dillon R. Biofluidmechanics of reproduction. In *Annual Review of Fluid Mechanics. Vol. 38*, Vol. 38, Annual Review of Fluid Mechanics. Annual Reviews: Palo Alto, CA, 2006; 371–394.
4. Fogelson AL, Guy RD. Platelet-wall interactions in continuum models of platelet thrombosis: formulation and numerical solution. *Mathematical Medicine and Biology—A Journal of the IMA* 2004; **21**:293–334.
5. Lim S, Peskin CS. Simulations of the whirling instability by the immersed boundary method. *SIAM Journal on Scientific Computing* 2004; **25**(6):2066–2083.
6. Miller LA, Peskin CS. A computational fluid dynamics study of 'clap and fling' in the smallest insects. *Journal of Experimental Biology* 2005; **208**(2):195–212.
7. Griffith BE. On the volume conservation of the immersed boundary method. *Communications in Computational Physics* 2012; **12**(2):401–432.
8. Griffith BE. Immersed boundary model of aortic heart valve dynamics with physiological driving and loading conditions. *International Journal for Numerical Methods in Biomedical Engineering* 2012; **28**(3):317–345.
9. Griffith BE, Luo R, McQueen DM, Peskin CS. Simulating the fluid dynamics of natural and prosthetic heart valves using the immersed boundary method. *International Journal of Applied Mechanics* 2009; **1**:137–177.
10. Griffith BE, Hornung RD, McQueen DM, Peskin CS. An adaptive, formally second order accurate version of the immersed boundary method. *Journal of Computational Physics* 2007; **223**(1):10–49.
11. Donea J. Arbitrary Lagrangian–Eulerian finite element methods. *Computational Methods for Transient Analysis*, North-Holland, Amsterdam, 1983.
12. Hughes TJR, Liu WK, Zimmermann TK. Lagrangian–Eulerian finite element formulation for incompressible viscous flows. *Computer Methods in Applied Mechanics and Engineering* 1981; **29**(3):329–349.
13. Heil M. An efficient solver for the fully coupled solution of large-displacement fluid–structure interaction problems. *Computer Methods in Applied Mechanics and Engineering* 2004; **193**(1-2):1–23.
14. Le Tallec P, Mouro J. Fluid structure interaction with large structural displacements. *Computer Methods in Applied Mechanics and Engineering* 2001; **190**(24-25):3039–3067.
15. Leuprecht A, Perktold K, Prosi M, Berk T, Trubel W, Schima H. Numerical study of hemodynamics and wall mechanics in distal end-to-side anastomoses of bypass grafts. *Journal of Biomechanics* 2002; **35**(2):225–236.
16. Quarteroni A, Tuveri M, Veneziani A. Computational vascular fluid dynamics: problems, models and methods. *Computing and Visualization in Science* 2000; **2**(4):163–197.
17. Quaini A, Quarteroni A. A semi-implicit approach for fluid–structure interaction based on an algebraic fractional step method. *Mathematical Models and Methods in Applied Sciences* 2007; **17**(6):957–985.
18. Baaijens FPT. A fictitious domain/mortar element method for fluid–structure interaction. *International Journal for Numerical Methods in Fluids* 2001; **35**(7):743–761.
19. Van Loon R, Anderson PD, De Hart J, Baaijens FPT. A combined fictitious domain/adaptive meshing method for fluid–structure interaction in heart valves. *International Journal for Numerical Methods in Fluids* 2004; **46**(5):533–544.
20. Fang H, Wang Z, Lin Z, Liu M. Lattice Boltzmann method for simulating the viscous flow in large distensible blood vessels. *Physical Review E* 2002; **65**(5):051925–1–051925–12.
21. Feng ZG, Michaelides EE. The immersed boundary-lattice Boltzmann method for solving fluid–particles interaction problems. *Journal of Computational Physics* 2004; **195**(2):602–628.
22. Krafczyk M, Cerrolaza M, Schulz M, Rank E. Analysis of 3D transient blood flow passing through an artificial aortic valve by lattice-Boltzmann methods. *Journal of Biomechanics* 1998; **31**(5):453–462.
23. Krafczyk M, Tölke J, Rank E, Schulz M. Two-dimensional simulation of fluid–structure interaction using lattice-Boltzmann methods. *Computers and Structures* 2001; **79**(22-25):2031–2037.

24. Cottet GH, Maitre E, Milcent T. Eulerian formulation and level set models for incompressible fluid–structure interaction. *ESAIM: Mathematical Modelling and Numerical Analysis* 2008; **42**:471–492.

25. Figueroa CA, Vignon-Clementel IE, Jansen KE, Hughes TJR, Taylor CA. A coupled momentum method for modeling blood flow in three-dimensional deformable arteries. *Computer Methods in Applied Mechanics and Engineering* 2006; **195**(41-43):5685–5706.

26. Gerbeau J, Vidrascu M. A quasi-Newton algorithm based on a reduced model for fluid–structure interactions problems in blood flows. *Mathematical Modelling and Numerical Analysis* 2003; **37**(4):631–648.

27. Nobile F, Vergara C. An effective fluid–structure interaction formulation for vascular dynamics by generalized Robin conditions. *SIAM Journal of Scientific Computing* 2008; **30**:731–763.

28. Zhao S, Xu X, Collins M. The numerical analysis of fluid-solid interactions for blood flow in arterial structures part 2: development of coupled fluid–solid algorithms. *Proceedings of the Institution of Mechanical Engineers, Part H* 1998; **212**:241–252.

29. Bazilevs Y, Calo VM, Hughes TJR, Zhang Y. Isogeometric fluid–structure interaction: theory algorithms and computations. *Computational Mechanics* 2008; **43**:3–37.

30. Bazilevs Y, Calo VM, Zhang Y, Hughes TJR. Isogeometric fluid–structure interaction analysis with applications to arterial blood flow. *Computational Mechanics* 2006; **38**(4-5):310–322.

31. Galindo M, Cervera M, Codina R. On the computational efficiency and implementation of block-iterative algorithms for nonlinear coupled problems. *Engineering with Computers* 1996; **13**:4–30.

32. Deparis S, Fernandez M, Formaggia L. Acceleration of a fixed point algorithm for a fluid–structure interaction using transpiration condition. *Mathematical Modelling and Numerical Analysis* 2003; **37**(4):601–616.

33. Fernández MA, Moubachir M. A Newton method using exact Jacobians for solving fluid–structure coupling. *Computers and Structures* 2005; **83**(2-3):127–142.

34. Matthies H, Steindorf J. Numerical efficiency of different partitioned methods for fluid–structure interaction. *Zeitschrift fur Angewandte Mathematik und Mechanik* 2000; **2**(80):557–558.

35. Causin P, Gerbeau JF, Nobile F. Added-mass effect in the design of partitioned algorithms for fluid–structure problems. *Computer Methods in Applied Mechanics and Engineering* 2005; **194**(42-44):4506–4527.

36. Michler C, Hulshoff SJ, van Brummelen EH, de Borst Rx. A monolithic approach to fluid–structure interaction. *Computers and Fluids* 2004; **33**:839–848.

37. Badia S, Nobile F, Vergara C. Fluid–structure partitioned procedures based on Robin transmission conditions. *Journal of Computational Physics* 2008; **227**(14):7027–7051.

38. Bukač M, Čanić S, Glowinski R, Tambača J, Quaini A. Fluid–structure interaction in blood flow capturing non-zero longitudinal structure displacement. *Journal of Computational Physics* 2012; **235**:515–541.

39. Bukač M, Čanić S. Longitudinal displacement in viscoelastic arteries: a novel fluid-structure interaction computational model, and experimental validation. *Mathematical Biosciences and Engineering* 2013; **10**(2): 295–318.

40. Guidoboni G, Glowinski R, Cavallini N, Čanić S. Stable loosely-coupled-type algorithm for fluid–structure interaction in blood flow. *Journal of Computational Physics* 2009; **228**(18):6916–6937.

41. Fernández MA. Incremental displacement-correction schemes for the explicit coupling of a thin structure with an incompressible fluid. *Comptes Rendus de l'Académie des Sciences Paris* 2011; **349**(7-8):473–477.

42. Fernández MA, Mullaert J. Displacement–velocity correction schemes for incompressible fluid–structure interaction. *Comptes Rendus de l'Académie des Sciences Paris* 2011; **349**(17-18):1011–1015.

43. Fernández MA. Incremental displacement-correction schemes for incompressible fluid–structure interaction: stability and convergence analysis. *Numerische Mathematik* 2012; **123**:21–65.

44. Fernández MA, Gerbeau JF, Grandmont C. A projection algorithm for fluid–structure interaction problems with strong added-mass effect. *Comptes Rendus Mathematique* 2006; **342**(4):279–284.

45. Astorino M, Chouly F, Fernández MA. An added-mass free semi-implicit coupling scheme for fluid–structure interaction. *Comptes Rendus Mathematique* 2009; **347**(1-2):99–104.

46. Astorino M, Chouly F, Fernández Varela MA. Robin based semi-implicit coupling in fluid–structure interaction: stability analysis and numerics. *SIAM Journal of Scientific Computing* 2009; **31**:4041–4065.

47. Badia S, Quaini A, Quarteroni A. Splitting methods based on algebraic factorization for fluid–structure interaction. *SIAM Journal of Scientific Computing* 2008; **30**(4):1778–1805.

48. Murea CM, Sy S. A fast method for solving fluid–structure interaction problems numerically. *International Journal for Numerical Methods in Fluids* 2009; **60**(10):1149–1172.

49. Deparis S, Discacciati M, Fourestey G, Quarteroni A. Fluid–structure algorithms based on Steklov–Poincaré operators. *Computer Methods in Applied Mechanics and Engineering* 2006; **195**(41-43):5797–5812.

50. Badia S, Nobile F, Vergara C. Robin–Robin preconditioned Krylov methods for fluid–structure interaction problems. *Computer Methods in Applied Mechanics and Engineering* 2009; **198**(33-36):2768–2784.

51. Burman E, Fernández MA. Stabilization of explicit coupling in fluid–structure interaction involving fluid incompressibility. *Computer Methods in Applied Mechanics and Engineering* 2009; **198**:766–784.

52. Hansbo P. Nitsche's method for interface problems in computational mechanics. *Gesellschaft für Angewandte Mathematik und Mechanik* 2005; **28**(2):183–206.

53. Muha B, Čanić S. Existence of a solution to a fluid-multi-layered-structure interaction problem. *Journal of Differential Equations* 2014; **256**:658–706.

54. Hundertmark-Zaušková A, Lukáčová-Medvid'ová M, Rusnáková G. Fluid–structure interaction for shear-dependent non-Newtonian fluids. In *Topics in Mathematical Modeling and Analysis*, Vol. 7, Jindřich Nečas Cent. Math. Model. Lect. Notes. MatfyzPress: Prague, 2012; 109–158.

55. Badia S, Nobile F, Vergara C. Fluid–structure partitioned procedures based on Robin transmission conditions. *Journal of Computational Physics* 2008; **227**:7027–7051.

56. Peskin CS, Miller LA. A computational fluid dynamics of 'clap and fling' in the smallest insects. *Journal of Experimental Biology* 2005; **208**:195–212.

57. Nobile F. Numerical approximation of fluid–structure interaction problems with application to haemodynamics. *Ph.D. Thesis*, EPFL, Switzerland, 2001.

58. Ma X, Lee GC, Wu SG. Numerical simulation for the propagation of nonlinear pulsatile waves in arteries. *Journal of Biomechanical Engineering* 1992; **114**:490.

59. Barker AT, Cai XC. Scalable parallel methods for monolithic coupling in fluid–structure interaction with application to blood flow modeling. *Journal of Computational Physics* 2010; **229**(3):642–659.

60. Čanić S, Lamponi D, Mikelić A, Tambača J. Self-consistent effective equations modeling blood flow in medium-to-large compliant arteries. *Multiscale Modeling and Simulation* 2005; **3**(3):559–596.

61. Mikelić A, Guidoboni G, Čanić S. Fluid–structure interaction in a pre-stressed tube with thick elastic walls I: the stationary Stokes problem. *Networks and Heterogeneous Media* 2007; **2**(3):397.

62. Glowinski R. Finite element methods for incompressible viscous flow. In *Handbook of Numerical Analysis*, Vol. 9, Ciarlet PG, Lions J-L (eds). North-Holland: Amsterdam, 2003.

63. Boiarkine O, Kuzmin D, Čanić S, Guidoboni G, Mikelić A. A positivity-preserving ALE finite element scheme for convection–diffusion equations in moving domains. *Journal of Computational Physics* 2011; **230**(8):2896–2914.

64. Farhat C, Geuzaine P, Grandmont C. The discrete geometric conservation law and the nonlinear stability of ALE schemes for the solution of flow problems on moving grids. *Journal of Computational Physics* 2001; **174**(2):669–694.

65. Hundertmark-Zaušková A, Lukáčová-Medvid'ová M, Rusnáková G. Kinematic splitting algorithm for fluid–structure interaction in hemodynamics. *Computer Methods in Applied Mechanics and Engineering* 2013; **265**:83–106.

66. Muha B, Čanić S. Existence of a weak solution to a nonlinear fluid—structure interaction problem modeling the flow of an incompressible, viscous fluid in a cylinder with deformable walls. *Archive for Rational Mechanics and Analysis* 2013; **207**(3):919–968.

67. Quaini A. Algorithms for fluid–structure interaction problems arising in hemodynamics. *Ph.D. Thesis*, EPFL, Switzerland, 2009.

68. Badia S, Quaini A, Quarteroni A. Modular vs. non-modular preconditioners for fluid–structure systems with large added-mass effect. *Computer Methods in Applied Mechanics and Engineering* 2008; **197**(49-50):4216–4232.

Research Article

A modular, operator-splitting scheme for fluid–structure interaction problems with thick structures

M. Bukač, S. Čanić, R. Glowinski, B. Muha and A. Quaini
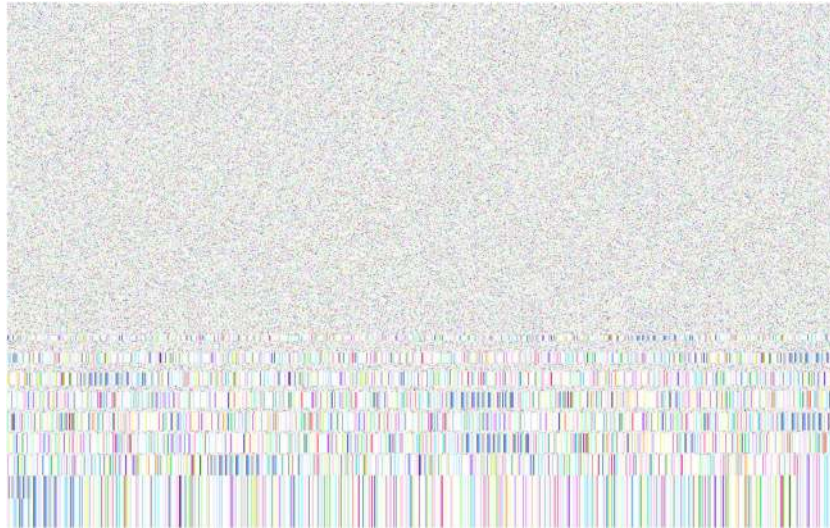
A novel stable, modular, operator-splitting scheme is presented for the simulation of fluid-structure interaction (FSI) problems in which the structure has finite thickness, comparable to the transverse dimension of the fluid domain. The fluid flow is modeled by the Navier-Stokes equations for an incompressible, viscous fluid, while the structure elastodynamics is governed by the equations of linear elasticity/viscoelasticity. Energy estimates associated with unconditional stability of the scheme are shown for the full, nonlinear FSI problem. Numerical examples show that this modular scheme compares well with monolithic schemes.